Structural control on volcanism in intraplate post collisional settings: Late Cenozoic to Quaternary examples of Iran and Eastern Turkey

Esmaeil Shabanian, Valerio Acocella, Anna Gioncada, Habibollah Ghasemi, Olivier Bellier

Structural control on volcanism in intraplate post collisional settings: Late Cenozoic to Quaternary examples of Iran and Eastern Turkey

Esmaeil Shabanian,[1] Valerio Acocella,[1,2] Anna Gioncada,[3] Habibollah Ghasemi,[4] and Olivier Bellier[1]

Received 7 October 2011; revised 2 April 2012; accepted 17 April 2012; published 6 June 2012.

[1] Volcanic activity focuses along plate boundaries. However, large volcanoes are also found in intraplate settings. For these volcanoes, geodynamic processes responsible for magma generation and structural controls on magma rise and extrusion need to be evaluated. We merge original (field and remote sensing) and available (geodetic, geophysical, and petrological) data to consider the tectono-magmatic relationships of three large intraplate volcanoes in the E-Anatolian-Iranian plateau; Sar'akhor (NE Iran), Damavand (Central Alborz) and Ararat (E Anatolia). In NE Iran, a Miocene-Pliocene NW-trending compression activated E-W dextral faults to the NW of Sar'akhor and N-S sinistral faults to the SE, creating an extruding wedge to the west of this volcano. Since Quaternary, NE-trending compression inverted fault movement, hindering further block extrusion and volcanism terminated. The adakitic composition of the Sar'akhor rocks suggests post-collisional melting of oceanic slab and/or mafic lower crust, possibly triggered by an asthenospheric rise after slab break-off or intramantle delamination. For the active Damavand and Ararat volcanoes, available data suggest magma generation due to rising hot asthenosphere, following lithospheric delamination or slab break-off in a transtensional environment. The features common to Sar'akhor, Damavand and Ararat allow proposing a model, where transtension focuses the rise of magma in intraplate settings overlying hot asthenosphere produced by delamination or slab break-off.

Citation: Shabanian, E., V. Acocella, A. Gioncada, H. Ghasemi, and O. Bellier (2012), Structural control on volcanism in intraplate post collisional settings: Late Cenozoic to Quaternary examples of Iran and Eastern Turkey, *Tectonics*, *31*, TC3013, doi:10.1029/2011TC003042.

1. Introduction

[2] Magmatism focuses along convergent and, to a lesser extent, divergent plate boundaries [e.g., *Sandwell et al.*, 2005]. However, several notable and volumetrically significant volcanoes are also found in intraplate settings. For most of these volcanoes, possible relations with hot spot activity or rising asthenosphere are proposed [see *Anderson and Schramm*, 2005, and references therein]; a minor portion of volcanoes has a more debated or unknown relationship with the overall tectonic setting [e.g., *Davidson et al.*, 2004; *Yokoyama et al.*, 2007].

[3] In general, two main types of uncertainties may be associated with the location of these intraplate volcanoes. The first concerns the definition of the general geodynamic processes responsible for the generation of magma [e.g., *Kay and Kay*, 1993; *Cañón-Tapia and Walker*, 2004; *White et al.*, 2006]. Melt availability is in fact the first fundamental requisite to explain magmatism. The melting should be induced by common mechanisms, such as the decompression due to rifting at divergent plate boundaries and/or the release of fluids/melts by a sinking slab at convergent plate boundaries; however, in intraplate settings other processes may also play a role. These usually consist of slab steepening, slab break-off, and lithospheric/intramantle delamination, as well as the upward suction of the mantle or retreatment of the lithosphere in W- or E-NE-directed subductions, respectively; all these processes result in the rise of asthenosphere replacing lithosphere [e.g., *Chalot-Prat and Girbacea*, 2000; *Şengör et al.*, 2003; *Doglioni et al.*, 2009; *Gioncada et al.*, 2010; *Ducea*, 2011]. The other uncertainty regards the definition of the structural control on the rise and extrusion of magma. This is commonly, but not exclusively, related to the activity

[1]CEREGE–UMR 7330, Aix-Marseille Université, and CNRS–Institut PYTHEAS, Technopôle de l'Environnement Arbois-Méditerranée, Aix en Provence, France.
[2]Dipartimento di Scienze Geologiche, Università Roma Tre, Rome, Italy.
[3]Dipartimento di Scienze della Terra, Università di Pisa, Pisa, Italy.
[4]Faculty of Geosciences, Shahrood University of Technology, Shahrud, Iran.

Corresponding author: E. Shabanian, CEREGE–UMR 7330, Aix-Marseille Université, BP80, F-13545 Aix en Provence, CEDEX 04, France. (shabanian@cerege.fr)

0278-7407/12/2011TC003042

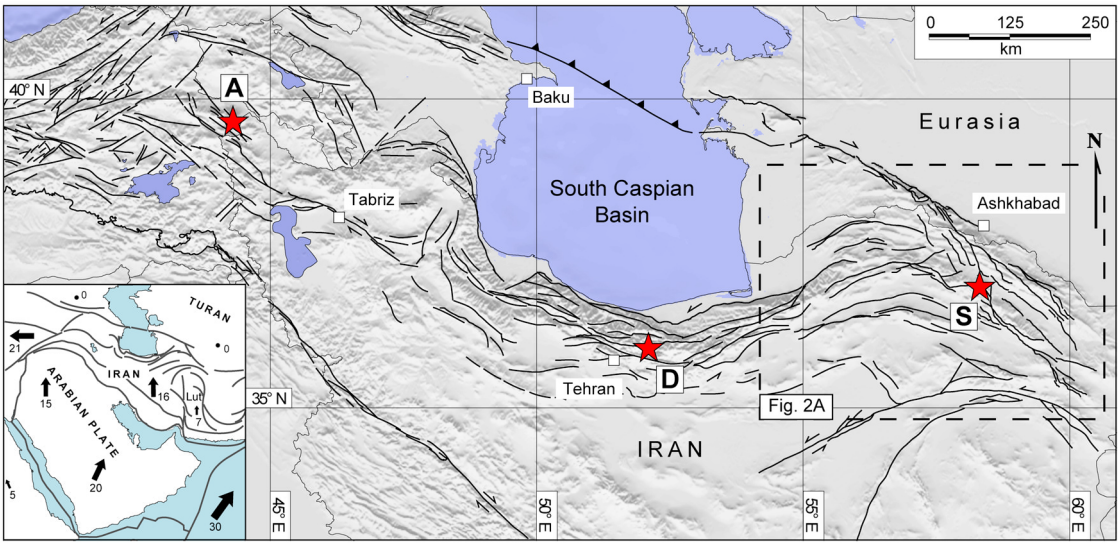

Figure 1. GTOPO30. Shaded relief image showing the location of Sar'akhor (S), Damavand (D), and Ararat (A) volcanoes in the northern part of the Arabia-Eurasia collision zone. Fault traces (black line) are after *Bozkurt* [2001], *Koçyigit et al.* [2001], *Jackson et al.* [2002], *Hessami et al.* [2003], *Shabanian et al.* [2010], and *Solaymani Azad et al.* [2011a]. Lower left inset shows the geodynamic setting of Arabia-Eurasia collision/subduction framework. Black arrows and associated numbers (in mm/yr) represent the present-day Arabia-Eurasia plate velocities after *Reilinger et al.* [2006].

of fault systems providing pathways for the rise and emplacement of magma [*Grocott et al.*, 1994; *McNulty et al.*, 1998; *Acocella and Funiciello*, 2010]. In intraplate settings, the location, activity and kinematics of the crustal structures possibly related to magmatism may not be straightforward [e.g., *Chalot-Prat and Girbacea*, 2000; *Riller et al.*, 2001; *Acocella et al.*, 2011, and references therein]. Therefore, only the knowledge of both the deeper geodynamic setting and the structure of the brittle crust may allow a proper understanding and explanation for volcanic activity. For example, the inferred location of Mt. Etna on the side of a rift zone [*Monaco et al.*, 1997] does not completely justify the localized and exceptional output rate, and additional, deeper mechanisms were invoked [*Gvirtzman and Nur*, 1999; *Doglioni et al.*, 2001].

[4] The Alpine-Himalayan collisional belt includes large intraplate volcanoes, possibly indirectly related to plate boundary convergence, but not located above active subducting slabs. Several of these volcanoes are active and located in the Turkish-Iranian plateau (Figure 1), such as Mt. Ararat (East Anatolia) and Mt. Damavand (Central Alborz) [*Yilmaz et al.*, 1998; *Mehdizadeh et al.*, 2002; *Davidson et al.*, 2004; *Liotard et al.*, 2008; *Kheirkhah et al.*, 2009, and references therein]. Other volcanoes are extinct, but still in the same tectonic setting [e.g., *Alberti et al.*, 1980; *Karakhanian et al.*, 2003; *Shabanian et al.*, 2009b], suggesting a persistence and continuity of intraplate magmatism also in the Late Cenozoic.

[5] This study tries to provide constraints to define the tectonic setting of intraplate volcanoes along the East Anatolia-Iranian portion of the Alpine-Himalayan collisional belt. To this aim, we (1) analyze the Miocene-Pliocene Sar'akhor volcano in NE Iran, using remote sensing, field and petro-chemical data, and (2) place it in a wider context, considering the features of the nearby active analogues (Mt. Ararat and Mt. Damavand), to better understand the possible tectono-magmatic processes in intraplate settings and to propose a general model for intraplate volcanoes in the Turkish-Iranian plateau.

2. Tectonic Setting of NE Iran and the Meshkan Area

[6] Late Mesozoic northward motion of Arabia with respect to Eurasia was partly associated with subduction under Central Iran, with collision between ~35 to 12 Ma [e.g., *Hessami et al.*, 2001; *Agard et al.*, 2005; *Vincent et al.*, 2005; *Guest et al.*, 2006; *Mouthereau et al.*, 2012, and references therein]. The Arabia-Eurasia convergence is accommodated at a rate of 26 ± 2 mm/yr at ~59°E [e.g., *Vernant et al.*, 2004; *Reilinger et al.*, 2006]. The Turkish–Iranian plateau (Figure 1) is not undergoing major crustal thickening [e.g., *Jackson et al.*, 1995; *McClusky et al.*, 2000], although earlier collision-generating thickening is indicated by both present Moho depths, ranging from 40 to 70 km [*Maggi et al.*, 2000; *Paul et al.*, 2006; *Radjaee et al.*, 2010], and post-middle Miocene contraction [e.g., *Allen et al.*, 2004; *Guest et al.*, 2006; *Mouthereau et al.*, 2007; *Morley et al.*, 2009]. The plateau has typical elevations of 1.5–2 km. The ongoing deformation is principally taken up by strike-slip faulting in NW Iran [e.g., *Talebian and Jackson*, 2002; *Copley and Jackson*, 2006; *Solaymani Azad et al.*, 2011b], Alborz [e.g., *Ritz et al.*, 2006], Zagros [e.g., *Authemayou et al.*, 2006], southern and eastern Iran [*Walker and Jackson*, 2004; *Regard et al.*, 2005; *Le Dortz et al.*, 2009; *Farbod et al.*, 2011] and Kopeh Dagh [e.g., *Shabanian et al.*, 2009a] (Figure 1). Shortening is currently focused on the Zagros (6.5 ± 2 mm/yr) and Alborz Mountains (8 ± 2 mm/yr) [*Vernant et al.*, 2004]. However, at the lithospheric scale, the plateau seems deformed over a broad area, with vertically coherent deformation [*Kaviani et al.*, 2009].

[7] The northward subduction of Tethyan oceanic crust beneath the Iranian microcontinent gave rise to the extensive Eocene volcanism in central and northern Iran [*Berberian and King*, 1981; *Berberian et al.*, 1982; *Bina et al.*, 1986; *Stampfli and Borel*, 2002; *Agard et al.*, 2005]. Since Oligocene, volcanism has been occurring intermittently [e.g., *Jahangiri*, 2007] and, since ~10 Ma, predominantly within the Turkish–Iranian plateau [e.g., *Berberian and Berberian*, 1981; *Keskin et al.*, 1998; *Azizi and Moinevaziri*, 2009, and references therein].

[8] The northeastern part of the Arabia-Eurasia collision zone lies in NE Iran, including the Kopeh Dagh and Allah Dagh–Binalud mountains. The NW-trending Kopeh Dagh Mountains form an active deformation domain separating Central Iran from Eurasia (Figure 2a). Mesozoic and Tertiary sediments of the Kopeh Dagh were folded into parallel, asymmetric NW trending folds during Oligo-Miocene compression [*Stöcklin*, 1968; *Afshar Harb*, 1979; *Lyberis and Manby*, 1999]. These folds are obliquely dissected by active NNW-trending right-lateral and ENE-trending left-lateral strike-slip faults [e.g., *Tchalenko*, 1975; *Afshar Harb*, 1979; *Shabanian et al.*, 2009a]. The Allah Dagh–Binalud Mountains (Figure 2a) form NW-trending Mesozoic paleoreliefs south of the Kopeh Dagh [e.g., *Afshar Harb*, 1979] that thrusts over the northern margin of Central Iran [*Alavi*, 1992]. The Binalud is a collection of the paleo-Tethys remnants, as well as middle and upper Mesozoic, and Cenozoic rocks deformed since pre-late Triassic [*Alavi*, 1992].

[9] The Kopeh Dagh and Allah Dagh-Binalud deformation domains are structurally connected by strike-slip faults bounding the triangular-shaped Meshkan area (approximately 70 × 70 × 100 km) (Figure 2) [*Shabanian et al.*, 2009b]. This is outlined by three fault systems in a triangular configuration [*Shabanian et al.*, 2009b]: (1) the E-W Farhadan Fault, on the northern margin, (2) the ~N-S Chakaneh Fault, at the eastern boundary between the Meshkan area and Binalud, and (3) the NW-trending Meshkan fault system, on the southeastern boundary with Central Iran (Figure 2b). The Cenozoic evolution of the Meshkan area started when an Eocene sedimentary basin formed within the Alborz-Kopeh Dagh Mesozoic highlands, due to vertical faulting along the Farhadan and Chakaneh boundary faults [*Shabanian et al.*, 2009b]. Subsequent episodic deformation/sedimentation stages occurred during the Eocene to the Miocene [*Amini and Khan-Nazer*, 2000; *Shabanian et al.*, 2009b]. Later, the Neogene tectonic activity was testified by Miocene to late Pliocene volcanism, and the onset of strike-slip faulting along the Chakaneh and the Farhadan faults [*Shabanian et al.*, 2009b]. The inversion of movement of these strike-slip faults was induced by a regional change, in NE Iran, in the Plio-Quaternary stress state (section 3). The passage from a NW- to a NE-trending $\sigma 1$ stress axis, corresponding to the paleostress and modern stress states, respectively [*Shabanian et al.*, 2010; *Javidfakhr et al.*, 2011a], induced active dextral shear along the Chakaneh Fault and active sinistral shear along the Farhadan Fault [*Shabanian et al.*, 2009b, 2010].

[10] Long-lasting (~40 to ~2.3 Ma) volcanism has affected both the Meshkan area and the Sabzevar ophiolitic belt, to the south (Figure 2) [*Lensch et al.*, 1977; *Spies et al.*, 1983; *Amini and Khan-Nazer*, 2000]. In the Sabzevar belt, volcanic activity started since Eocene (~40 Ma) and continued to the end of Pliocene (~2.3 Ma). To the NE of the belt, volcanic activity has been localized in a small area (20 × 40 km) between the Sabzevar ophiolitic complex and the Neyshabur fault system, without further post-ophiolitic volcanics. Farther north, the Meshkan triangle is the only area affected by the Neogene volcanism within the Allah Dagh – Binalud Mountains (Figure 2b). The ages of volcanic rocks decrease northward, toward the Meshkan area [e.g., *Spies et al.*, 1983]. Except for some small volcanoes and dikes, most volcanic activity was concentrated in the northern part of the Meshkan area (Figures 2b and 3), and characterized by a few Neogene volcanoes, of which polygenetic Sar'akhor is by far the largest (~30 km in diameter; Figure 2b). Sar'akhor is composed of andesitic to dacitic pyroclastics rocks of Late Miocene to Late Pliocene, which overlie an olivine basaltic to basaltic lava base emplaced on the folded Eocene and Oligo-Miocene rocks [*Amini and Khan-Nazer*, 2000]. Previous studies [e.g., *Spies et al.*, 1983; *Bauman et al.*, 1983] suggested that a 100–150 km wide magmatic arc was created by the northward subduction (Cretaceous-Paleocene) of the steeply dipping slab of the Sabzevar Ocean, which was definitively closed in the Eocene. The subduction of this Tethyan seaway [e.g., *Shojaat et al.*, 2003] resulted in the formation of the Sabzevar ophiolitic and metamorphic belt, followed by the post-ophiolitic Eocene to Late Pliocene volcanism [e.g., *Lensch et al.*, 1977; *Spies et al.*, 1983; *Shojaat et al.*, 2003]. However, as subduction ended in the Late Paleocene [*Lensch et al.*, 1977; *Delaloye and Desmons*, 1980; *Spies et al.*, 1983] the Neogene volcanism in the area cannot be simply explained by dehydration of a subducting slab. The spatial distribution of the Neogene volcanoes localized in the Meshkan area also needs to be explained; the surface expression of the Sabzevar subduction remnant, which is ~200 km in length and ~10 km in width, implies widespread volcanism along the strike of the belt.

3. Tectono-Magmatic Features of the Meshkan Area

[11] In this section original and, subordinately, published structural, volcanological and petro-chemical information on the Meshkan area are provided, in order to reconstruct the possible tectono-volcanic relationships in the area.

3.1. Structural Features

3.1.1. Structural Analyses of Neogene Dikes

[12] Dikes are sub-vertical magma-filled fractures propagating in a direction normal to the minimum principal stress $\sigma 3$ [e.g., *Muller and Pollard*, 1977; *Nakamura et al.*, 1977; *Zoback and Zoback*, 1980; *Delaney et al.*, 1986; *Mount and Suppe*, 1992; *Bosworth and Strecker*, 1997]. Analysis of dike swarms yields the direction of the horizontal projection of either the maximum ($\sigma 1$) or intermediate ($\sigma 2$) principal stress, which is parallel to the dike orientation [*Nakamura*, 1977].

[13] In the Meshkan area, dike swarms and single dikes with different length (0.5–3 km), thickness (from a few meters to ~60 m) composition (dacite and alkaline mafic rocks; Table 1), and age (post Eocene to pre Pliocene) intrude the late Eocene and Oligocene rocks (Figures 2b and 3) [*Spies et al.*, 1983; *Ghaemi et al.*, 1999; *Amini and Khan-Nazer*, 2000]. Detailed mapping based on SPOT5 satellite

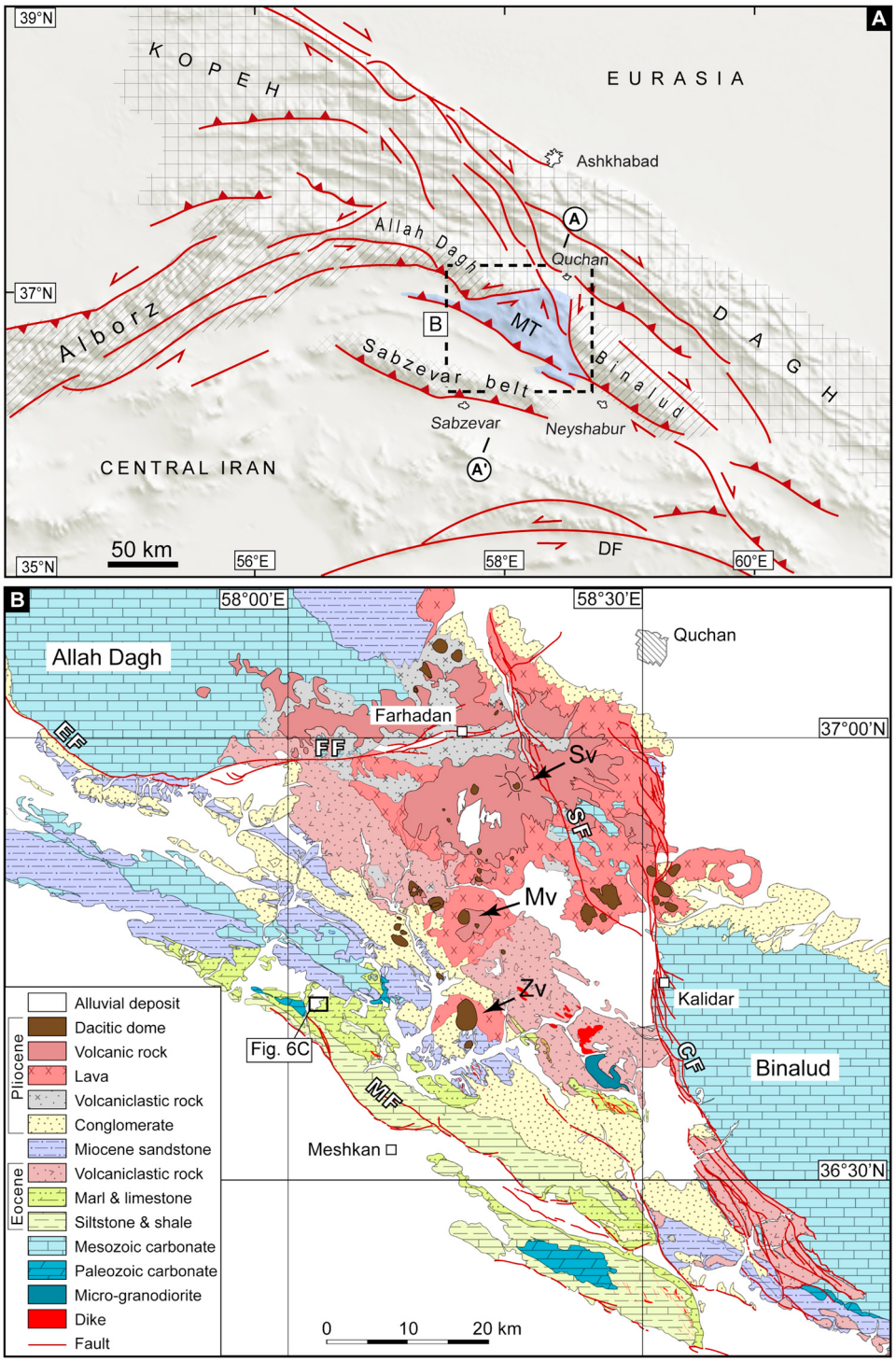

Figure 2. (a) Tectonic setting of the Meshkan triangle (MT) in NE Iran. Shaded image is based on GTOPO30 digital topographic data, and fault traces (red line) are after *Shabanian et al.* [2010]. DF, Doruneh Fault. A–A′ shows the location of Figure 5d. (b) Simplified geological map of the Meshkan area (modified after *Shabanian et al.* [2009b]). Abbreviations are faults and volcanoes: CF, Chakaneh Fault; FF, Farhadan Fault; MF, Meshkan fault system; SF, Sar'akhor Fault; Mv, Mahrokh-Kuh; Sv, Sar'akhor; Zv, Zohan.

imageries allowed us to determine the 2D-geometry of the dike segments. These are typically sub-vertical, with a preferred orientation throughout the middle and southern part of the region (Figure 3). The orientation of each dike was measured and analyzed using non-weighted rose diagrams (Figure 3a). All the dikes strike consistently N146 ± 10°, regardless of their size and composition. Given that the youngest NW-trending dikes intrude Oligocene rocks, their

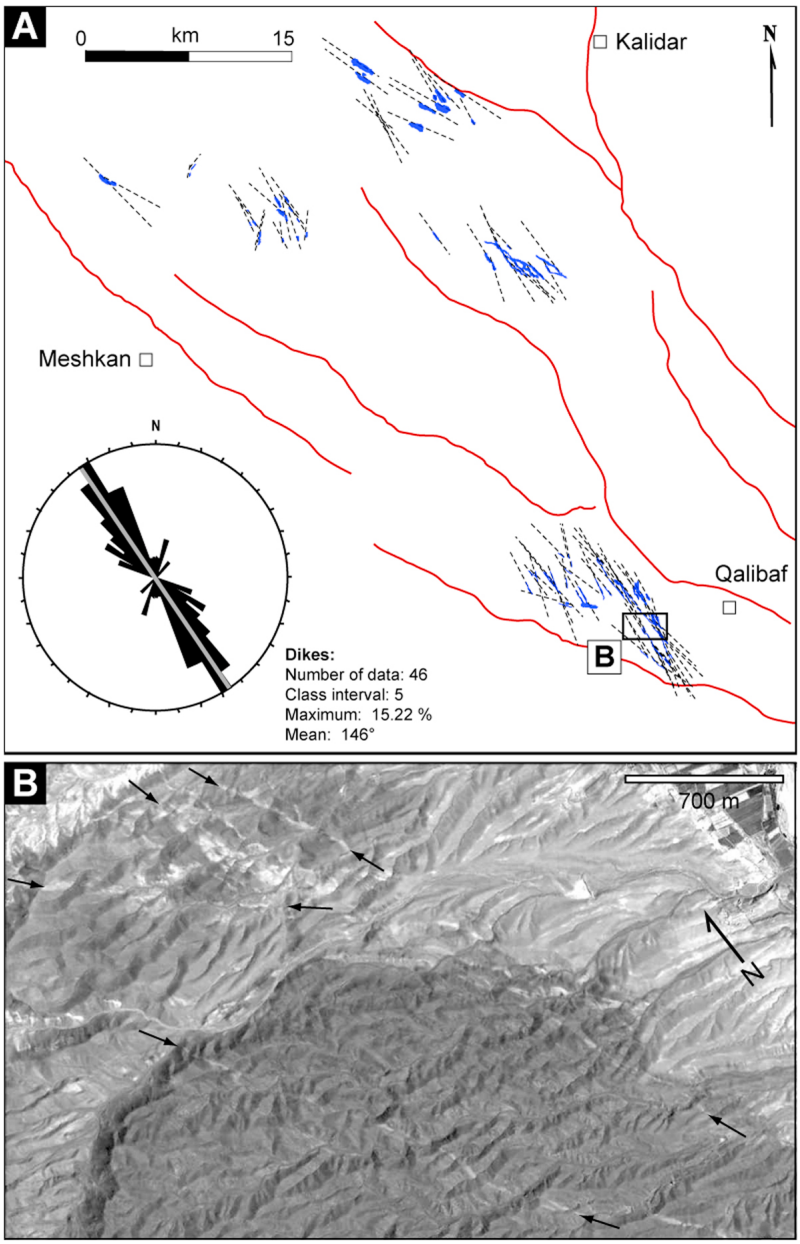

Figure 3. (a) Map of Miocene-Pliocene dikes (blue closed polygons) affecting the southeastern part of the Meshkan area. Dashed lines indicate orientation of dikes. Preferred orientation (~N146°E) of the dikes is shown by the lower left rose diagram. (b) QuickBird image (Google Earth), showing dikes intruded the Eocene-Oligocene rocks in the southeast of the Meshkan area (see Figure 3a for the location).

predominant orientation suggests a Neogene NE-trending minimum horizontal stress axis (σ_{hmin}), and a NW-oriented maximum horizontal compression (σ_{hmax}) affecting the area during their emplacement. Such a stress pattern is consistent with the direction of the principal paleostress axes ($\sigma 1$ = N140 ± 10°, σ_{hmin} = N50 ± 10°) determined from the inversion analysis of fault kinematic data in NE Iran, including the study area [*Shabanian et al.*, 2010] (see also section 3.1.3).

3.1.2. Volcano Elongation

[14] Volcanoes and related structural features have commonly been used as paleostress indicators [e.g., *Feraud and Campredon*, 1983; *Bosworth and Strecker*, 1997]. In particular, volcano elongation and alignment are widely used stress indicators [e.g., *Fiske and Jackson*, 1972; *Nakamura*, 1977; *Jackson and Shaw*, 1975; *Feraud et al.*, 1980; *Bosworth et al.*, 2003].

[15] Various volcanic landforms, such as volcanoes, domes and calderas are well-developed in the Meshkan area (Figures 4 and 5). Most of these features, especially volcanic domes, show a preferred elongation, in map view. To study the possible relationships to the regional stress, a detailed mapping of these domes has been carried, and the best fit

Table 1. Major (weight %) and Trace (ppm) Elements Compositions of Selected Meshkan Samples[a]

Sample	T4-2	FM.3	FM.29	T14-5	T6-2	T2-2	T-10	FM.6	T5-5	T5-13	T14-4	T10-5	T10-1	T12-12	T13-3	A8	FM.35	FM.10	T7-5	T13-8	FM.17
SiO_2 (wt %)	50.52	50.97	51.00	52.76	60.89	61.33	61.45	62.66	63.87	66.34	66.48	66.65	67.66	68.08	68.50	68.60	68.77	68.97	69.21	69.56	70.83
TiO_2	1.16	1.11	1.20	1.56	0.69	0.58	0.65	0.66	0.43	0.45	0.59	0.34	0.35	0.27	0.23	0.48	0.35	0.27	0.16	0.23	0.25
Al_2O_3	19.14	18.15	17.83	19.27	18.67	18.51	18.06	17.36	19.96	17.27	18.90	17.52	18.43	17.34	16.55	18.77	16.14	16.67	15.51	16.71	16.04
Fe_2O_3tot	8.67	9.32	9.85	5.49	4.19	9.89	5.45	5.69	2.22	2.71	0.42	3.24	1.30	2.09	3.35	3.06	3.51	2.65	5.89	2.45	2.66
MnO	0.11	0.15	0.18	0.17	0.06	0.02	0.04	0.06	0.02	0.05	0.05	0.05	0.05	0.04	0.04	0.00	0.06	0.06	0.00	0.04	0.05
MgO	6.88	5.83	5.70	5.12	3.62	0.35	1.85	1.78	2.39	2.69	0.76	1.35	1.46	0.93	0.68	0.08	1.36	0.84	0.27	0.69	0.65
CaO	7.81	7.54	7.27	9.40	4.80	3.78	6.02	5.54	3.67	4.54	3.43	4.66	4.63	4.71	4.03	0.33	4.25	3.67	0.42	3.69	3.44
Na_2O	3.77	5.03	4.59	3.87	4.23	3.61	4.14	4.39	6.59	4.70	4.71	4.16	4.09	4.51	4.39	5.83	3.81	4.61	5.03	4.48	4.19
K_2O	1.51	1.26	1.66	1.84	2.54	1.72	2.03	1.50	0.71	1.07	4.40	1.92	1.88	1.75	2.12	2.83	1.63	2.11	3.46	2.06	1.77
P_2O_5	0.44	0.65	0.73	0.52	0.31	0.21	0.31	0.37	0.15	0.17	0.26	0.12	0.13	0.27	0.11	0.02	0.12	0.16	0.06	0.10	0.12
LOI	2.4	1.1	1.0	2.9	2.0	0.4	0.9	1.5	2.2	0.9	1.7	0.9	2.3	1.8	1.5	2.8	1.0	2.0	1.5	3.4	0.7
Ba	304	275	320	579	460	439	493	410	436	491	476	672	569	439	409	502	430	460	285	323	490
Co	28.2	32	31	16	12.9	9.5	3.1	15	6.5	3.6	7	1.8	10.9	9.5	7	3.3	8	7	4	9.1	5
Cs	5.7	0.73	0.77	0.2	1.6	0.9	0.6	0.98	0.7	1	0.5	0.4	0.9	0.9	0.7	0.8	0.67	0.76	0.2	0.7	8
Ga	15.6	-	-	16.1	16.1	16.4	16	-	15.6	15.9	15.8	14.5	17.3	16.4	16.3	16.6	-	-	15	14.6	-
Hf	4	7.2	6.3	4.2	4.3	4.5	3	6.4	2.9	2.9	3.2	4	3.4	4.5	2.9	2.9	5.9	7	3.6	3.7	6.9
Nb	20	26	22	22.1	20.9	22.2	7	15	10	8.1	24.4	26.4	16	22.2	10.6	8.2	7	9	14.6	14.4	7.5
Rb	26.9	40	37	57.6	46.3	44.9	39.3	38	43.5	44.7	66.4	58.7	31.8	44.9	44.8	43.5	41	43	16.9	32.4	47
Sr	570	820	850	463	564	469	443	440	516	470	364	270	710	469	508	488	500	458	490	512	455
Ta	1.2	0.81	0.87	1.4	1.3	1.5	0.5	0.72	0.9	0.6	2.5	2.3	1.1	1.5	-	0.6	0.91	0.78	1.1	1.1	0.68
Th	3.9	3.5	3.6	9.3	9.5	11.1	4.9	11	7	5.1	12.8	-	7.9	11.1	7	4.5	5.5	4.8	10	10.3	5
U	1	-	-	2	2.1	2	1.4	-	1.9	1.6	3.7	2.8	1.6	2	2.1	1.6	-	-	2.5	2.6	-
V	142	150	125	98	82	61	19	85	41	21	44	14	68	61	45	18	21	25	60	61	29
W	0.5	-	-	1	1.8	1.1	0.5	-	0.7	0.5	1.2	0.9	0.8	1.1	7	0.5	-	-	0.5	8	-
Zr	171.8	137	120	166.8	169.1	170.9	105.7	121	99.5	95	111.4	147	126.6	170.9	104	98.1	132	138	134.4	133.1	140
Y	21.2	22	24	16.1	14.9	14.2	5.8	16	7.2	7.5	11.8	9.8	9.4	14.2	8.1	8	6.5	5	13.4	13.3	6
La	23.8	32	32	36	32.6	27.5	18.1	28	19.3	17.9	28.9	23.1	30.2	27.5	19.3	19.4	18	17	21	26	20
Ce	48.9	61	55	59.6	57.1	49.5	31.5	49	31.5	31.7	48.3	35.5	52.8	49.5	33.6	34.1	34	30	41.4	44.1	33
Pr	5.6	-	-	6.19	6.12	5.44	3.31	-	3.43	3.37	5.05	3.42	5.54	5.44	3.64	3.6	-	-	4.52	4.72	-
Nd	20.5	25	27	20.8	21.6	20.1	11.4	18	11.5	11.5	16.9	11	18.5	20.1	12.9	12.6	11.5	10.3	15.6	16.3	12
Sm	4.08	5.5	5	3.5	3.63	3.37	1.85	3.2	1.93	1.95	2.67	1.76	2.91	3.37	2.15	2	2.2	1.85	2.52	2.79	2
Eu	1.37	1.63	1.62	1.03	1.03	0.95	0.52	1	0.6	0.53	0.72	0.6	0.96	0.95	0.63	0.6	0.64	0.55	0.68	0.76	0.7
Gd	3.98	4.5	4	3.07	3.19	3.27	1.5	3.2	1.67	1.69	2.38	1.61	2.54	3.27	1.84	1.82	1.85	1.2	2.5	2.62	1.5
Tb	0.66	0.56	-	0.52	0.49	0.5	0.2	-	0.25	0.24	0.36	0.27	0.36	0.5	0.27	0.26	-	-	0.39	0.4	-
Dy	3.76	3.9	4	2.69	2.73	2.7	1.04	2.8	1.29	1.27	2.01	1.56	1.79	2.7	1.42	1.37	1.3	0.9	2.3	2.23	1.0
Ho	0.76	-	-	0.55	0.53	0.52	0.19		0.27	0.24	0.4	0.32	0.34	0.52	0.28	0.26	-	-	0.47	0.47	-
Er	2.1	2.3	2.3	1.52	1.52	1.42	0.52	1.6	0.72	0.66	1.13	0.98	0.92	1.42	0.79	0.69	0.7	0.5	1.31	1.28	0.46
Tm	0.34	-	-	0.28	0.25	0.23	0.08	-	0.13	0.11		0.15	0.14	0.23	0.12	0.11	-	-	0.21	0.21	-
Yb	2	2.2	2	1.52	1.54	1.37	0.52	-	0.72	0.64	1.31	1.11	0.88	1.37	0.77	0.65	0.46	0.37	1.35	1.39	0.35
Lu	0.32	-	-	0.26	0.23	0.21	0.08	-	0.12	0.1	0.2	0.19	0.14	0.21	0.12	0.11	-	-	0.21	0.22	-
Mo	1.7	-	-	0.3	1.7	0.1	0.03	-	1.2	0.3	1	0.1	0.6	0.1	1.2	0.1	-	-	0.1	0.2	-
Cu	5.2	-	-	19.4	13	11.3	6.5	-	22.5	6.1	8.6	2.9	13.4	11.3	20.3	4.1	-	-	1.4	3.3	-
Pb	1.3	-	-	1	4.8	4.2	0.9	-	0.4	0.6	16.7	2.1	1.4	4.2	0.7	0.6	-	-	0.7	5.3	-
Zn	43	-	-	41	33	32	5	-	26	6	39	11	11	32	25	6	-	-	6	29	-
As	2	-	-	2.6	10.8	1.5	0.6	-	0.5	0.5	0.5	5	1	1.5	0.5	0.5	-	-	2.7	2.3	-
$(La/Yb)_{cn}$	8.1	9.9	10.9	16.1	14.4	13.6	23.6	-	18.2	19.0	15.0	14.1	23.3	13.6	17.0	20.3	26.6	31.2	10.6	12.7	38.8
Sr/Y	27	37	35	29	38	33	76	28	72	63	31	28	76	33	63	61	77	92	37	39	76

[a]The data are originally presented in Persian by *Ghasemi et al.* [2010]. $Fe_2O_{3\ total}$: all Fe recalculated as Fe_2O_3. $(La/Yb)_{cn}$: chondrite-normalized La/Yb, after *McDonough and Sun* [1995].

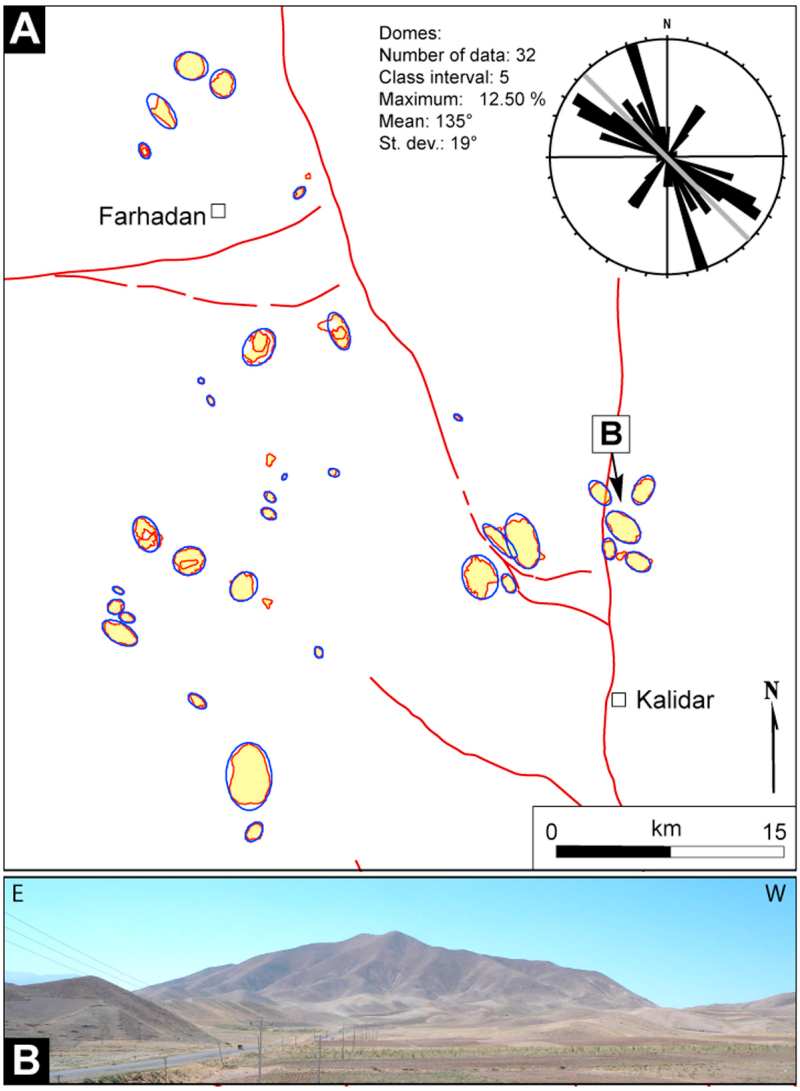

Figure 4. (a) Simplified map of volcanic landforms of the Meshkan area, surrounded by best fit ellipses (blue), analyzed in this study. The upper right weighted rose diagram (see text for more information) shows the preferred orientation of the elliptical volcanic landforms. (b) Field photograph of a volcanic dome. The location of the photograph is marked in Figure 4a.

ellipses, with different flattening, are plotted over each landform (Figure 4).

[16] The flattening f, where $f = (L_M - L_m)/L_M$ (L_m and L_M are the minor and major axis of the ellipse approximating the base of the dome in map view, respectively), was used to weight the statistical analysis of the orientation data in rose diagrams (Figure 4). The flattening values obtained for volcanic landforms were divided by the smallest value into normalized flattening values. Then, the orientation data has been weighted by related normalized flattening values. That is, rather than each elongation datum contributing equally to the final result, more flattened ellipses are adjusted to contribute more than others. In the resulted rose diagrams, thus, the predominant direction is representative of the preferred orientation of most elliptical landforms. The elongated axes of these elliptical volcanic landforms trend between N115° to N160°, with a mean orientation of N135 ± 20°. The more dispersed orientation of domes with regard to dikes could be explained by (1) the elliptical geometry of the domes that are less precise in the orientation analysis than linear dikes, and (2) external factors, including the initial slope of the dome base, controlling its overall elongation. Nevertheless, the mean orientation of N135 ± 20° is consistent with the predominant orientation (N146 ± 10°) of the dikes, and lies around the geologically determined paleostress $\sigma 1$ axis [*Shabanian et al.*, 2010] (see section 3.1.3). This suggests that the magma intruded along fissures parallel to the maximum horizontal paleostress axis $\sigma 1$, to form domes with a preferred NW-SE orientation. The emplacement of such domes at 2.5 ± 0.5 Ma [*Spies et al.*, 1983; *Shabanian et al.*, 2009b; *Ghasemi et al.*, 2010] implies a NW-SE compression up to Late Pliocene.

3.1.3. Paleostress State and Kinematic Changes Along the Boundary Faults

[17] Fault kinematic data (fault planes and associated striations, with well-known slip sense) measured in NE Iran often

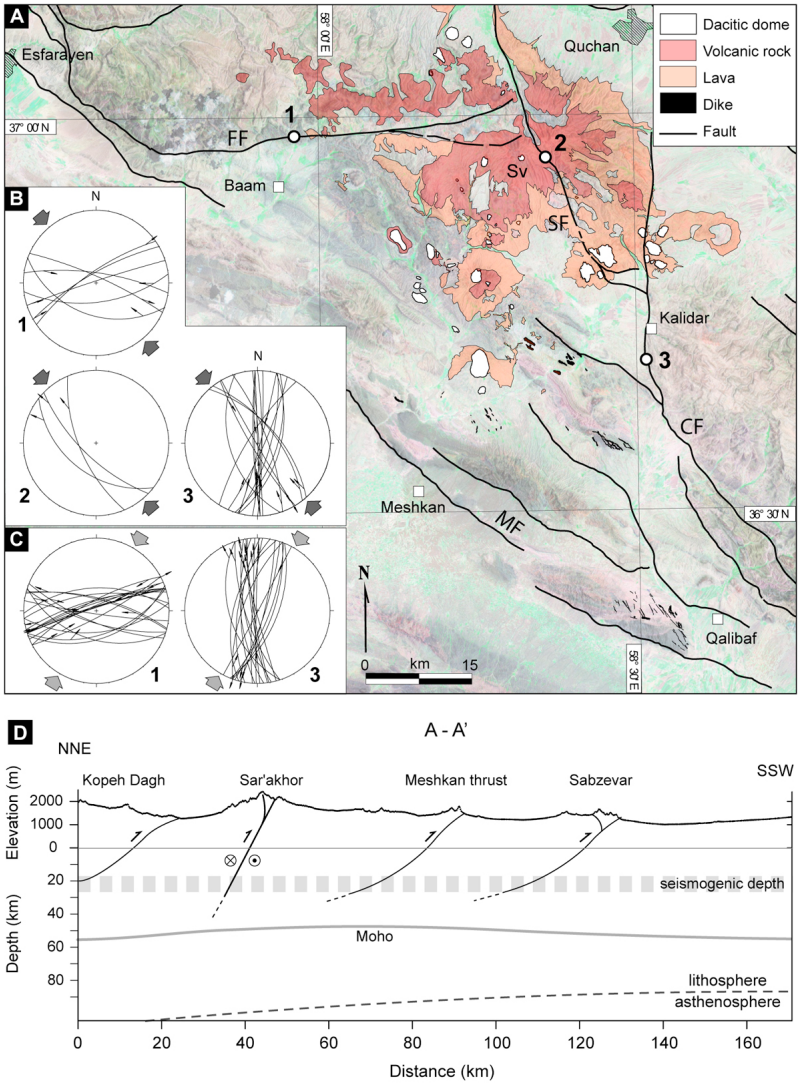

Figure 5. (a) Simplified volcano-tectonic map of the Meshkan area, indicating the boundary faults and the Sar'akhor volcano (Sv). Numbers on boundary faults refer to diagrams shown in Figures 5b and 5c, abbreviations as in Figure 2b. (b and c) Stereoplots of fault kinematic data (fault planes and their associated striation) measured along the boundary faults (numbers on Figure 5a) indicating the kinematics of fault during the NW-SE paleostress and NE-SW modern stress compressions, respectively. (d) Idealized scheme of the lithospheric configuration of the Meshkan area. The thickness of seismogenic layer is based on *Maggi et al.* [2000]. The "inferred" lithosphere/asthenosphere boundary and Moho depth are based on *Shad Manaman et al.* [2011]. See Figure 2a for the location of cross-section.

show multiple sets of striations [*Shabanian et al.*, 2009b, 2010], revealing a multiphase tectonic history (Figures 5b and 5c). The distinction between sets of striations on the same fault plane has been done directly on the field, on the basis of the crosscutting relationships, in order to properly reconstruct the tectonic history of the region [see *Shabanian et al.*, 2010]. This approach indicates that two main stress directions occurred in NE Iran during the Neogene: a first NW-trending paleostress compression and a second NE-trending modern compression. While this tectonic variation was previously described [*Shabanian et al.*, 2010] its effects on the main tectonic structures and the magmatic evolution of the area are considered in this study for the first time (Figure 6).

[18] On the northern border of the Meshkan triangle, along the WSW-trending Farhadan Fault and other parallel faults, the initial right-lateral slip changed into the present-day left-lateral slip (Figure 6). On the E border of the Meshkan triangle, the initially left-lateral N-S faults parallel to the Chakaneh Fault are presently reactivated as right-lateral strike-slip faults (Figure 6). Similarly, the southern part of the area is affected by nearly parallel NNW-trending strike-slip faults that cut and displace Eocene and Miocene folded rocks; stratigraphic markers along the faults were left-laterally displaced (Figure 6c). In the present-day tectonic context, the NNW-trending faults are right-lateral [e.g., *Tchalenko*, 1975; *Afshar Harb*, 1979; *Shabanian et al.*, 2009a, 2009b, 2010]. In addition, earlier transtensional faulting along NNW-trending

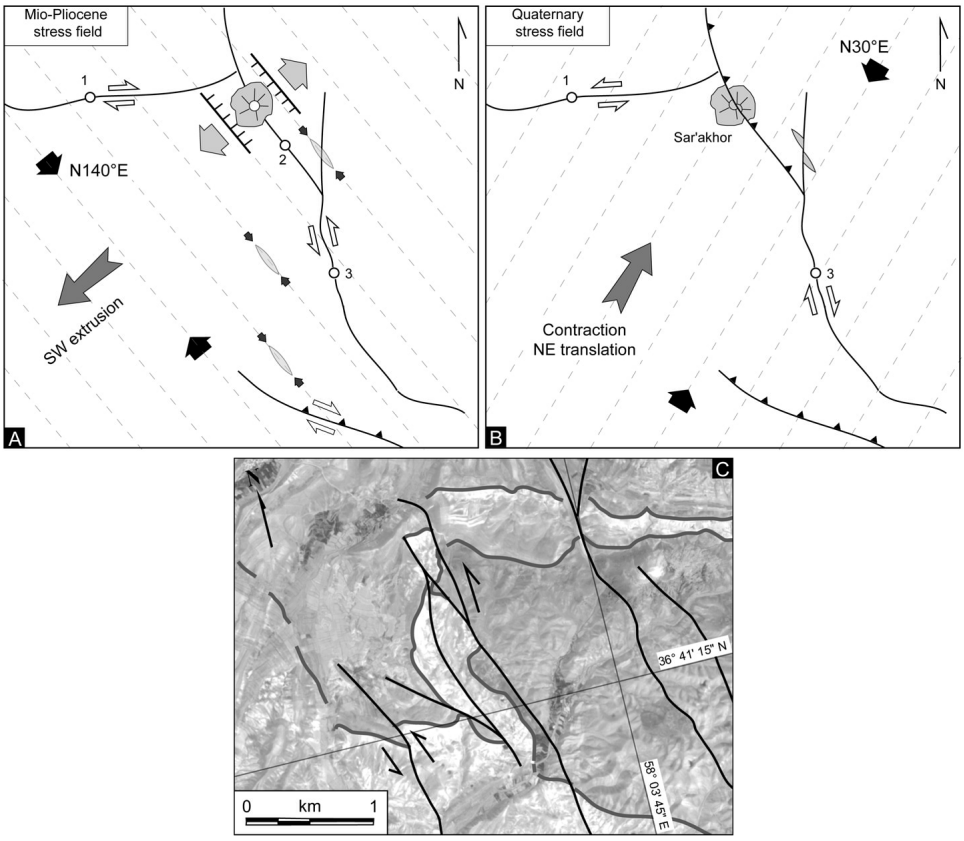

Figure 6. Idealized models illustrating the tectonic evolution of the Meshkan area. (a) Southwest extrusion of the Meshkan triangle and volcanic activity localized in Sar'akhor volcano. Almond-shaped polygons are opening fissures parallel to the NW-SE compression. (b) Tectonic inversion in the area after the change in stress from the NW- to NE-trending compressions by Late Pliocene. The motion on faults has been inverted and some volcanic domes have right-laterally been displaced along the eastern boundary fault. Numbers on faults refer to fault kinematic data presented in Figures 5b and 5c. (c) A series of nearly parallel NNW-trending strike-slip faults that cut and left-laterally displace stratigraphic markers of Eocene and Miocene ages. See Figure 2b for the location.

faults, such as the Sar'akhor Fault has changed into the current transpressional faulting. Applying the NW-trending paleostress $\sigma 1$ axis to the NW-trending faults implies that the present-day pure reverse faults at the southern boundary of the Meshkan area had mainly been right-lateral faults (Figure 6). More in general, the stress change resulted in the inversion of the previously active strike-slip tectonic regime within the Meshkan triangle (Figure 6). Given the geometry of the faults bounding the Meshkan area, left-lateral faulting along the Chakaneh Fault and right-lateral displacement along the Farhadan Fault during the NW-trending $\sigma 1$ caused southwestward extrusion of the Meshkan triangular area (Figure 6). Such a motion could have produced local extension at the northern corner of the Meshkan triangle, where Sar'akhor volcano is located, enhancing decompression, partial melting and volcanism.

[19] There is no constraint on the age of this kinematic change in NE Iran [see *Shabanian et al.*, 2010, and references therein]. But, *Shabanian et al.* [2009b] show that a NW-trending elliptical volcanic dome dated at ~2.4 Ma has been right-laterally offset along the N-S Chakaneh Fault. Assuming that the dome was formed during the paleostress activity (NW-trending $\sigma 1$), its subsequent right-lateral displacement along the N-S Chakaneh Fault suggests a maximum age of ~2.4 Ma for the change in the Plio-Quaternary stress state. Also, the amount of total displacement along the boundary faults during the activity of paleostress state is unclear. However, the restoration of both geomorphic and geological markers offset along the Farhadan (~7 km left-laterally) and Chakaneh (~6 km right-laterally) faults since the establishment of the present-day tectonic regime [*Shabanian et al.*, 2009b] implies ~8 km of northeastward translation of the Meshkan triangle after the tectonic inversion. Several studies document a similar, but sometimes diachronous drastic change in the late Cenozoic tectonic regime of north and northeast Iran [see *Shabanian et al.*, 2010, and references therein]. This change may be due to the onset of northward subduction of the South Caspian Basin, and/or changes in the structural configuration or lithospheric characteristics of N and NE Iran during an evolving collisional convergence. At the moment, the cause of this tectonic change remains unclear.

3.2. Compositional Features of the Meshkan Magmatism and Sar'akhor Volcano

[20] Sar'akhor volcano is the most significant Miocene – Pliocene magmatic product in the Meshkan area. Today, the

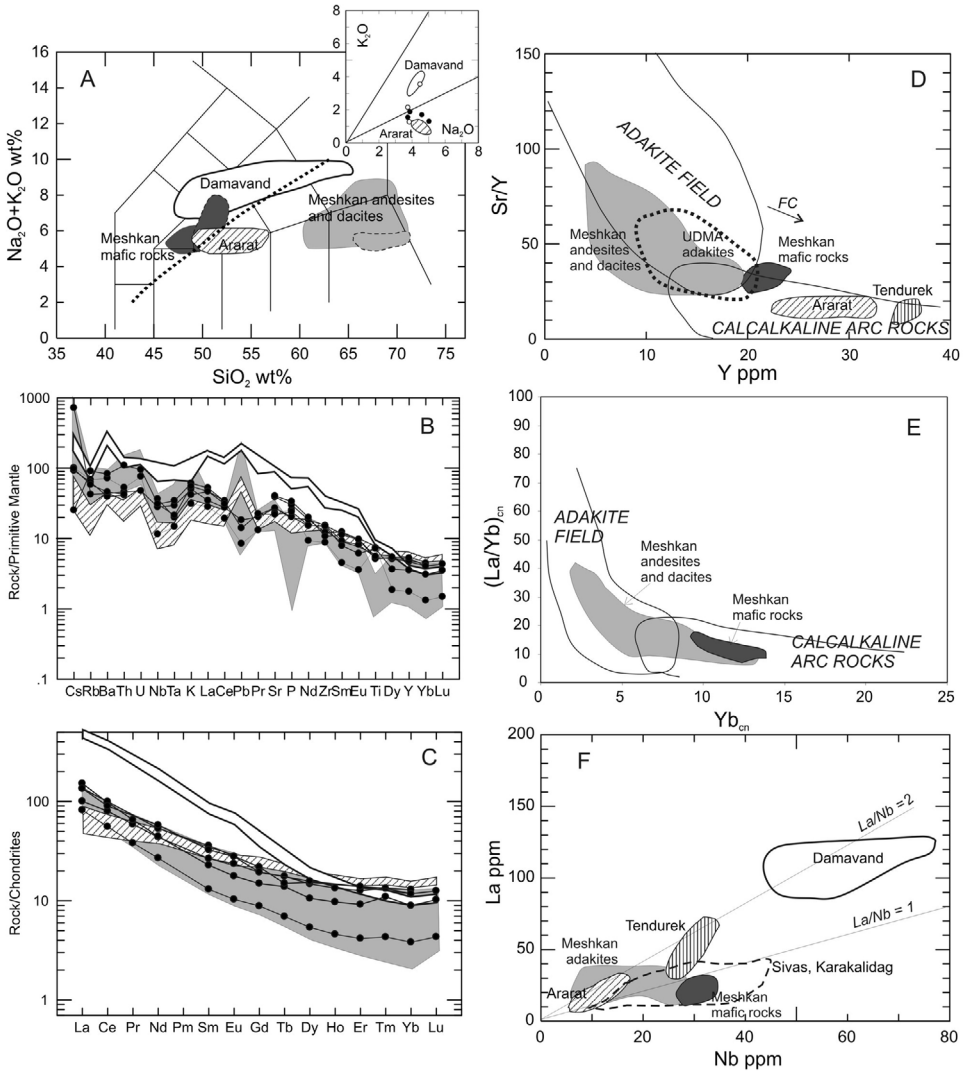

Figure 7. (a) Total alkali-silica diagram for Ararat, Damavand and Meshkan region rocks showing different subalkaline to moderately alkaline characters of the rocks. For Meshkan rocks, dashed polygon outlines data in *Spies et al.* [1983]; solid contour shows data in Table 1. The inset shows the Na_2O/K_2O ratio only for rocks with MgO > 4 wt%. Dots, Meshkan mafic rocks in Table 1; open circles, mafic rocks in *Spies et al.* [1983]. (b) Primitive mantle-normalized trace element patterns for the Meshkan andesite and dacite rocks (gray field) and Meshkan mafic rocks (dots); mafic rocks from Damavand (white field) and Ararat (dashed field) are also shown. (c) Chondrite-normalized REE patterns for the Meshkan, Damavand and Ararat rocks; symbols as in Figure 7b; normalization factors for Figures 7b and 7c after *Sun and McDonough* [1989]. (d and e) Sr/Y versus Y and $(La/Yb)_{cn}$ versus Yb_{cn} diagrams, respectively, showing the adakite signature of the Meshkan andesitic and dacitic rocks. FC, fractional crystallization. (f) La versus Nb diagram showing the high incompatible elements content of Damavand rocks [*Mehdizadeh et al.*, 2002; *Mirnejad et al.*, 2010] compared with Ararat [*Kheirkhah et al.*, 2009] and Meshkan rocks (Table 1); also, the higher La/Nb of Damavand compared with Meshkan mafic rocks and OIB-like Sivas and Karakalidag magmatism.

volcano is significantly eroded, and only its mid to lower portion is preserved, with a diameter of ~30 km (Figure 2b) and an altitude of nearly 2500 m, i.e., a height of ~800 m from its base. The volcano represents the last relevant magmatic episode in the Meshkan area. *Spies et al.* [1983] and *Bauman et al.* [1983] report age and compositional data of the volcanic rocks in the region between Quchan and Sabzevar, including the Meshkan area. They highlight the presence, in the last 40 Ma, of subalkaline andesites to dacites, with calc-alkaline affinity, and of mafic alkaline rocks (Figure 7a); the dacite rocks occur as isolated plugs, domes and dykes intruding andesitic rocks. The andesites (mainly pyroclastics, with few lava banks) and dacites range in age from 41 ± 2.1 to 2.7 ± 0.2 Ma becoming younger northward, reaching Late Miocene to Late Pliocene ages in the Meshkan area. Three individual samples from mafic alkaline rocks are dated between 26.2 ± 1.3 and 18.5 ± 0.9 Ma. The Sr isotopic ratios, corrected for age, are 0.7040–0.7057 for andesite and dacite rocks, and 0.7037–0.7057 for mafic rocks [*Bauman et al.*, 1983]. *Spies et al.* [1983]

interpret the dacite and andesite magmas as related to partial melting in the mantle wedge, following the post collisional detachment of the downgoing oceanic plate; partial melting at greater depths caused the alkaline magmas.

[21] *Ghasemi et al.* [2010] presented a petrographic and geochemical study of the Meshkan rocks based on a new set of samples (Table 1). K/Ar age estimates of these rocks range from 19.5 ± 0.5 to 2.29 ± 0.08 Ma. The composition of the analyzed samples confirms the presence of both andesite-dacite and mafic alkaline rocks, which have been reported by *Spies et al.* [1983] (Figure 7a). In the diagrams showing the concentration of primitive mantle-normalized elements (Figure 7b), all andesite and dacite samples display negative anomalies in Nb-Ta, P and Ti; anomalies in Pb are positive or negative. The mafic samples show similar negative anomalies in Nb-Ta, but, no anomalies in P and Ti. In chondrite-normalized REE diagrams (Figure 7c), andesite and dacite rocks show variably fractionated patterns, with $(La/Yb)_{cn}$ between 10 and 40, and no Eu anomaly. Similar patterns, but with $(La/Yb)_{cn}$ between 10 and 20, are observed in the mafic samples.

[22] The trace element and Sr isotope features of the Meshkan mafic rocks suggest that their primary magmas may have originated from an isotopically heterogeneous source [e.g., *Chalot-Prat and Girbacea*, 2000; *McCann et al.*, 2010, and references therein], probably, due to an older subduction (Paleotethys oceanic plate) under the Binalud Mountains [e.g., *Alavi*, 1996] resulting in a metasomatized mantle beneath the Meshkan area.

[23] As regards the andesite and dacite rocks, the geochemical data as a whole do not favor a derivation of those magmas from the Meshkan mafic magmas through differentiation processes involving fractional crystallization, in agreement with *Spies et al.* [1983]. The high Sr/Y (20–90), low Y (<20 ppm) and high $(La/Yb)_{CN}$ of most andesite and dacite samples suggest an adakitic character for these volcanic rocks (Figures 7d and 7e) [see *Drummond and Defant*, 1990]. These low Y, low Yb (<2 ppm), high La/Yb, high Sr, as well as the silicic character and the low $^{87}Sr/^{86}Sr$ of some samples (down to 0.7040) are in agreement with an origin of the magmas by partial melting of a garnet-bearing, plagioclase-free source, which could be represented by the metamorphosed basalts of an oceanic crust forming the slab (possibly as old as Variscan) foundering after the cessation of subduction [*Ghasemi et al.*, 2010]. The slab melts could have interacted with the metasomatized mantle wedge, thus explaining the trace elements patterns and the variable $(^{87}Sr/^{86}Sr)_i$. However, according to the low MgO wt% of these rocks, the interaction with the mantle peridotite was moderate. The as high as 0.7057 Sr isotopic ratios of some dacites could also be explained by contamination with crustal material; the latter should not have been volumetrically negligible, given the relatively high Sr content of these rocks. This is supported by the presence of crustal enclaves (gneiss, siltstone, marl and pelite) in the Meshkan andesitic to dacitic volcanic rocks [*Ghasemi et al.*, 2010]. Additional data, especially Nd and Pb isotope data, may better constrain the slab melting model and the possible involvement of sediments, mantle peridotite and crustal components.

[24] In the evaluation of the slab melting process, it has been suggested that the oceanic crust may undergo melting if still warm, that is younger than about 20 Ma, and slowly subducted [*Peacock et al.*, 1994]. Instead, some of the adakite rocks in the Meshkan area have been dated at only 2.4 ± 1.0 Ma [*Shabanian et al.*, 2009b; *Ghasemi et al.*, 2010], and may not be easily related to the generation of magma by partial melting of the slab. In addition, several works have suggested the difficulty for low fractions of melts above a slab to reach the surface, as these react with the mantle rocks and may get rapidly absorbed [e.g., *Chalot-Prat et al.*, 2010; *Topuz et al.*, 2011, and references therein]. Alternatively, recent experimental works and geochemical modeling have shown that the trace element features of adakitic compositions may be produced by a number of petrogenetic processes [see *Castillo*, 2012 for a review], including melting in the lower mafic portion of a thickened crust, leaving garnet as a residue [e.g., *Stern*, 2002; *Macpherson et al.*, 2006; *Chiaradia et al.*, 2009]. In the Meshkan area, the crust is currently 48–50 km thick (Figure 6d) [*Shad Manaman et al.*, 2011] and the base of the crust is not too distant from the pyrope garnet stability field [see *Topuz et al.*, 2011, and references therein]. Therefore, this scenario may also be plausible and could explain the crustal isotopic signature of most of the Meshkan adakites.

[25] The long-lasting eruption of the Meshkan adakitic magmas implies the generation of the adakitic melts more than 20 Ma after the cessation of the Sabzevar subduction (Late Paleocene) [*Lensch et al.*, 1977; *Delaloye and Desmons*, 1980; *Spies et al.*, 1983]. To explain such a time gap and the prolonged generation of adakitic melts, either by slab or mafic lower crust melting, a temperature perturbation induced by a hot asthenospheric upflow is required. Several models, which are not mutually exclusive, may be envisaged.

[26] The upflow of asthenospheric mantle could be due to post-collisional slab break-off; this would enhance melting of slab portions during a prolonged period after cessation of the subduction. Such a process has been inferred for the emplacement of adakite magmas during the post-collisional activity of the nearby Urumieh-Dokhtar magmatic arc, in Late Miocene [*Jahangiri*, 2007] and Plio-Quaternary [*Khodami et al.*, 2009]. Partial melting of the slab may also be occurring by adiabatic decompression when the detached slab becomes warmer and positively buoyant in the upper mantle due to conductive heating [e.g., *Green et al.*, 2001]. However, both the continental and oceanic lithospheres seem to be lighter than the asthenosphere, particularly if serpentinized [e.g., *Kelly et al.*, 2003], preventing to generalize the slab break-off scenario.

[27] Another possibility to explain the upwelling of hot asthenosphere is a post-collisional thinned continental lithosphere, due to intramantle delamination [e.g., *Chalot-Prat and Girbacea*, 2000]. Alkaline rocks, erupted between 15 and 2 Ma in Central Iran, west of the Lut block [*Saadat et al.*, 2010], were also interpreted to signal a lithospheric delamination process [see also *Al-Lazki et al.*, 2004] that allowed the asthenosphere uprise. This is in agreement with (1) the anomalous hot and/or thin mantle lid under Central Iran, inferred from the broad Pn low-velocity anomalies [*Al-Lazki et al.*, 2004], and (2) the upper mantle S-velocity structures across the Iranian plateau [*Shad Manaman et al.*, 2011], which indicate low-velocity overriding material beneath Central Iran. The Meshkan area lies at the northern boundary of this low-velocity zone. Thus, interpreting the

magma of the Meshkan area as resulting from the Central Iran delamination should not be excluded.

[28] Finally, discussing mantle wedge asymmetries versus the polarity of subduction zones, *Doglioni et al.* [2009] suggested that similar magmatic events may be generated along the retrobelt of orogens by the upward suction of the mantle beneath the end-member E- or NE-directed subduction zones [see also *Doglioni et al.*, 1999, 2007]. Nevertheless, the steeply dipping character of the Sabzevar oceanic slab [*Spies et al.*, 1983], the N-directed polarity of the subduction zone, and the ~25 Ma time gap between the end of subduction and the volcanism in the Meshkan area (discussed above) may have not provided optimal conditions for the upward suction of the mantle.

[29] In summary, among several existing models, the hypotheses of slab detachment and/or lithospheric delamination may better explain the upflow of asthenospheric mantle and temperature perturbation, and consequently, the long-lasting magmatism in the Meshkan area. Nevertheless, the present knowledge of the mantle structure beneath the Meshkan area does not allow us to discriminate between these hypotheses.

3.3. Volcanological Features of Sar'akhor Volcano

[30] The former height of the Sar'akhor volcanic edifice was reconstructed to evaluate both its size and productivity, and eventually, to compare these parameters with analogues currently observed in the Arabia-Eurasia collision zone. To estimate the paleo-height of Sar'akhor volcano, we use two distinct and original methods based on (1) the dip of volcanic deposits, and (2) the overall rock composition.

[31] According to the first method, good exposures of the volcano base are found on its northern flank. Here, repeated measurements of the attitude of the deposits constituting the base of the volcano were taken from satellite image of the volcano superposed on SRTM digital topographic data (Google Earth and GeoMapApp software). Along a ~5-km-wide zone on the north and northeast flanks of the volcano, at a mean altitude of 2100 m, the dip of these deposits is constantly ~20°. The strike of stratified volcanic deposits slightly changes from E-W on the north flank to NW-SE on the northeast flank, highlighting a tangential configuration (Figure 8). Using the horizontal distance of the deposits from the inferred summit, the height of the volcano above the mean altitude of the measurement points can be inferred through the linear extrapolation of the dip of these deposits toward the summit (Figure 8). There are two candidates for the former volcano summit; the "present summit" located to the east of the Sar'akhor Fault, and the inferred "eroded summit" located to the west of the fault (Figure 8), at the respective mean horizontal distances of ~3.5 and ~8.9 km from the deposits (Figure 8). The NE side of the NE-dipping Sar'akhor Fault has been displaced upwards of ~110 m [*Shabanian et al.*, 2009b], forming the "present summit" (~2510 m); this is higher than the "eroded summit" (~2440 m). Interestingly, the continuation of the dip-direction of the two domains of deposits defines an elliptical area in which the former summit is expected to lie (Figure 8). The present summit is on the northern border of the ellipse, and the eroded summit, after the restoration of the ~3 km right-lateral displacement of the Sar'akhor Fault [*Shabanian et al.*, 2009b], locates in the western corner of the ellipse (Figure 8b). As both possibilities are plausible, our estimate for the height of volcano incorporates both the ~3.5 and ~8.9 km horizontal distances of the deposits from the possible former summits, as lower and upper bounds, respectively. This yields an additional height between ~1200 and ~3050 m above the 2100 m mean altitude of the measurement points; that is, the volcano reached an initial altitude between ~3300 and ~5150 m above sea level (Figure 8). Given that the base of the Sar'akhor volcano is presently located at ~1700 m, the edifice is expected to have been 2500 ± 900 m high. Such an estimate, even though far from being precise, relies on the assumption that the dip of the deposits maintains constant toward the summit. However, in most stratovolcanoes the dip of the deposits increases toward the summit, and the volcanoes commonly show a concave-upward profile. So, this mean estimated value has to be considered as a minimum.

[32] For the second method, we evaluated a general relationship between the composition of the volcano and the overall shape of the edifice. For this purpose, we considered the SiO_2 content (in weight %) of the magmas, taken as representative of their viscosity, plotted against the aspect ratio A (height/width) of the volcanic edifice. We compiled these data for fourteen polygenetic volcanic edifices worldwide, with a morphology ranging from mafic shield volcanoes to steep felsic stratovolcanoes (Figure 9). Despite the large variability in the SiO_2 content shown by some volcanoes, there is an evident proportional relationship with the aspect ratio, showing how steeper volcanoes are characterized by rocks with higher mean SiO_2 contents (Figure 9). No detailed mineralogical study exists on Sar'akhor volcano; however, field evidence indicates the same rocks types as the domes and volcanic centers in the area (e.g., Markuh [*Ghasemi et al.*, 2010]). In addition, *Spies et al.* [1983] reported similar andesitic to dacitic characteristics for the Miocene - Pliocene volcanics throughout the area. Accordingly, we suggest an andesite to dacite composition with adakite characteristics for Sar'akhor rocks, and a mean SiO_2 content similar to other stratovolcanoes in the Meshkan area (60 ± 10% weight; Table 1) corresponding to an aspect ratio of ~0.12 in the diagram in Figure 9. Considering the present diameter of the Sar'akhor edifice (~30 km), we estimate its former height, above the basement, at ~3600 m.

[33] In summary, the two independent estimates allow reconstructing the former height of the Sar'akhor volcanic edifice, above its base, in the order of 3000 ± 900 m. This value implies that the volcano, characterized by a relevant height, had significant productivity in an intraplate collisional setting.

[34] Several Neogene polygenetic volcanoes, responsible for the emission of calc-alkaline to ultrapotassic orogenic rocks or, more in general, intraplate-type rocks, are found in the Turkish-Iranian Plateau [e.g., *Spies et al.*, 1983; *Aftabi and Atapour*, 2000; *Kheirkhah et al.*, 2009; *Ahmadzadeh et al.*, 2010]; of these, the Miocene - Pliocene Sar'akhor is the easternmost. Current nearby analogues of Sar'akhor, sharing an overall similar collisional intraplate setting and size, are Ararat (Northeast Anatolia) and Damavand (Central Alborz) volcanoes (Figure 1c). In the section below, the comparison of Ararat and Damavand volcanoes to Sar'akhor allows getting more insights on the development of these large individual intraplate edifices.

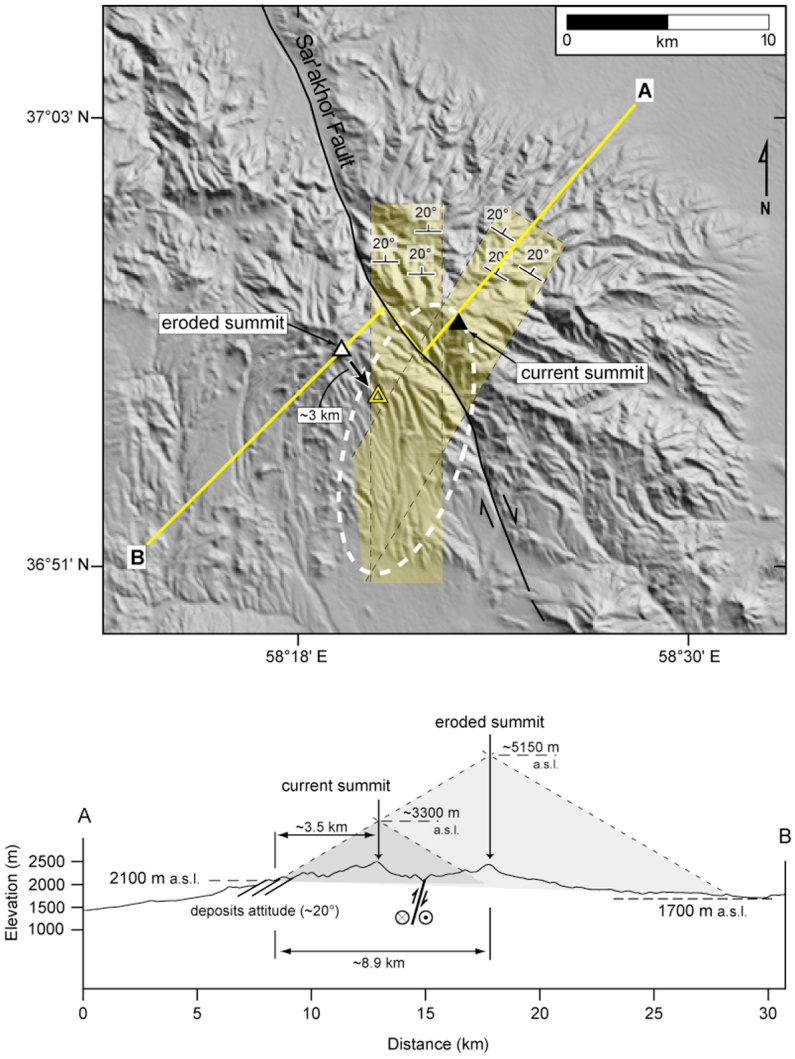

Figure 8. Geometric reconstructions of the paleo-height of Sar'akhor volcano by extrapolating the dip (~20°) of the deposits toward the current and inferred eroded summits. Ellipse marks the intersection zone between the two domains of deposit attitudes (light yellow bound). Yellow triangle shows the location of the eroded summit after the restoration of ~3 km right-lateral offset along the Sar'akhor Fault [*Shabanian et al.*, 2009b]; see text for details. A–B in the lower part is a topographic profile across Sar'akhor volcano after the restoration of ~3 km dextral offset. Shaded relief image is based on SRTM digital topographic data.

4. Overview of the Tectono-Magmatic Features of Ararat and Damavand Volcanoes

4.1. Tectono-Magmatic Features of Ararat Volcano

[35] Several active volcanoes in NE Anatolia and NW Iran are responsible for Holocene eruptions, the latter of which from Mt. Ararat in 1840 [*Yilmaz et al.*, 1998; *Karakhanian et al.*, 2002, 2004; *Kheirkhah et al.*, 2009] (Figure 1). Active volcanism in this region includes fields with monogenetic cones (Porak, Vaoyts-sar, Smbatasar, Tskhouk, and Maku), large calderas (Nemrut), shield volcanoes (Tendurek), composite volcanoes and stratovolcanoes (Süphan, Ararat) [*Yilmaz et al.*, 1998; *Karakhanian et al.*, 2002, 2004; *Kheirkhah et al.*, 2009]. Ararat is the largest active volcano in NE Anatolia and NW Iran. Ararat is a calc-alkaline, polygenic, compound stratovolcano [*Yilmaz et al.*, 1998] rising more than 4 km above the surrounding plains, reaching an altitude of 5165 m. The volcano consists of two major edifices: the Greater Ararat (5165 m) and the Lesser Ararat (3925 m), to the southeast. The distribution of parasitic cones and the main fissure eruptions on the flanks of the volcano highlight a preferred NW-SE alignment [*Karakhanian et al.*, 2002]. This reflects the trend of the major NW-SE trending structures in the area, with a predominant dextral motion [*Dewey et al.*, 1986] stable over the last ~5 Ma [*Copley and Jackson*, 2006]. These dextral faults develop several pull-apart structures and control volcanic activity [*Karakhanian et al.*, 2002 and 2004]. Mt. Ararat lies on the NW portion of a large (320 × 80 km) transtensional relay zone comprising several pull-apart structures controlled by NW-striking dextral faults, such as the Sardarapat Fault [e.g., *Karakhanian et al.*, 2002, 2004], and the North Tabriz Fault [*Berberian and Arshadi*, 1976; *Berberian and Yeats*, 1999; *Hessami et al.*, 2001; *Solaymani Azad*, 2009] at the northern and

Stratovolcano	SiO_2 (%)	A(H/W)	Reference
Damavand	57±7	0.11	Liotard et al. (2008)
Ararat	58±10	0.11	Kheirkhah et al. (2009)
Tendurek	52±6	0.05	
Etna	53±3	0.09	Corsaro et al. (2002)
Erta Ale	49±1	0.09	Barberi et al. (1980)
Dama Ale	49±1	0.03	
Terevaka	52±3	0.04	Vezzoli and Acocella (2009)
Kilauea	49±2	0.03	Tilling et al. (1987)
Hekla	53±7	0.08	Moune et al. (2007)
Vesuvio	57±5	0.09	Santacroce (1987)
Fuji	58±8	0.12	Takada et al. (2007), and ref.
Mount St. Helens	68±9	0.16	Blundy et al. (2008)
Mayon	64±12	0.15	McDormott et al. (2005)
Karymskii	62±7	0.17	Grib et al. (2009)

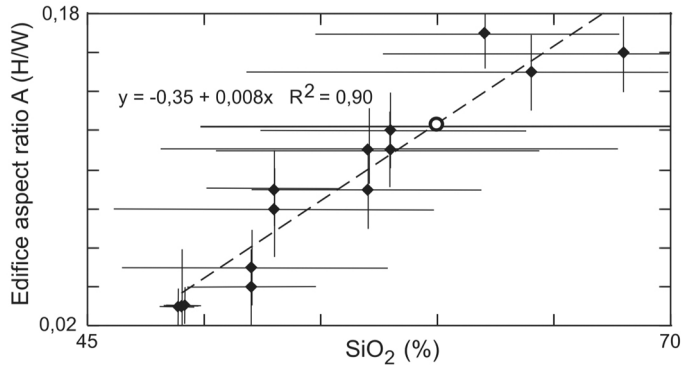

Figure 9. Compositional method to reconstruct the paleo-height of Sar'akhor volcano, based on the mean SiO_2 (wt %) content of the magma associated with different volcanic edifices with certain aspect ratio A (A = height H/width W of edifice). The table lists the data. The diagram relates the SiO_2 content of the volcanoes to their A. White circle shows the resulting inferred A of Sar'akhor. See text for details.

southern extremities, respectively. In particular, below Ararat, the Maku Fault ends into a transtensional horsetail structure made of ~NNW-striking splays branching from the main structure [e.g., *Karakhanian et al.*, 2002, 2004]. Such a structural pattern is inferred to control both the location of the Greater and Lesser Ararat volcanoes, and the preferred alignment of the parasitic cones [*Karakhanian et al.*, 2002, 2004].

[36] The Ararat rocks are trachybasalts and andesites (Figure 7a). The trachybasalts are slightly ne-normative, have $K_2O < 1$ wt% and rather low LILE content compared with the other volcanoes of the Turkish-Iranian plateau (e.g., Figure 7b), and have moderately high LILE/HFSE. The interpretation of the magmatic activity in the region is complex, due to the variety of magmatic types, including calc-alkaline, intraplate-type rocks [*Kheirkhah et al.*, 2009] and ultrapotassic rocks [*Ahmadzadeh et al.*, 2010]. The models to explain the genesis of these different magmas are mainly based on geophysical evidence indicating hot and partially molten asthenospheric material close to the base of the crust under eastern Turkey. The Moho depth varies between 30 and 55 km and the lithosphere is anomalously thin (60–80 km) [*Gök et al.*, 2003; *Al-Lazki et al.*, 2003; *Angus et al.*, 2006; *Tabatabai et al.*, 2008]. This indicates that the lithospheric mantle is absent, and that the asthenospheric mantle is directly located beneath the crust [*Al-Lazki et al.*, 2003]. Such a lithospheric structure suggests that the uplift of the plateau results from compensation of lithospheric thinning by the asthenospheric mantle, rather than crustal thickening [e.g., *Al-Lazki et al.*, 2003; *Copley and Jackson*, 2006]. This structure is in agreement with a post collisional process of delamination of lower lithosphere portions [e.g., *Pearce et al.*, 1990; *Keskin et al.*, 1998; *Maggi and Priestley*, 2005], rather than break-off of the subducted oceanic slab [*Keskin*, 2003, 2007; *Şengör et al.*, 2003; *Kheirkhah et al.*, 2009], to allow hot asthenospheric material replacing mantle wedge portions. *Lei and Zhao* [2007] favor the slab-break-off hypothesis through teleseismic tomography; however, a geophysically imaged slab-like structure may also result from mantle delamination, as reported in the southern Carpathians [*Chalot-Prat and Girbacea*, 2000].

[37] *Kheirkhah et al.* [2009] have explained the REE patterns and Y contents of the Ararat magmatism by partial melting in a thin lithospheric mantle at depths shallower than the garnet stability field. The LILE/HFSE values imply that the lithospheric mantle had been modified by elements carried by fluids/melts mobilized during subduction. The partial melting of the lithospheric mantle after the onset of Arabia-Eurasia collision has been related to the detachment of slab, which is inferred as the most plausible mechanism for the uprise of hot asthenosphere [*Dilek*, 2006; *Kheirkhah et al.*, 2009, and references therein].

4.2. Tectono-Magmatic Features of Damavand Volcano, Central Alborz

[38] Damavand is an intraplate composite stratovolcano in Central Alborz (Figures 10 and 11) [e.g., *Brousse and Moine*

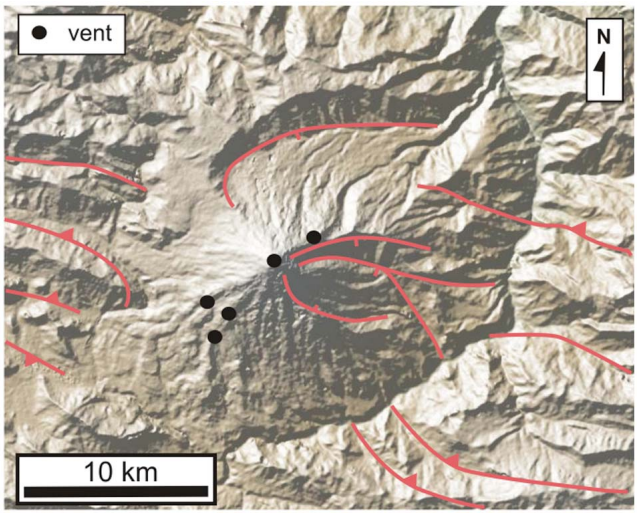

Figure 10. Schematic structural map of the Damavand volcano highlighting faults and the main fracture systems (red lines) and vents (black dots). Underlying DEM kindly provided by GeoMapApp (http://www.geomapapp.org).

Vaziri, 1982; *Davidson et al.*, 2004]. The Alborz Mountains surround the oceanic crust of the South Caspian Basin [e.g., *Berberian*, 1983; *Jackson et al.*, 2002; *Allen et al.*, 2003a]. Alborz has undergone a complex evolution, including various compressional episodes separated by extensional phases [e.g., *Stöcklin*, 1968, 1974; *Berberian and King*, 1981; *Berberian*, 1983; *Alavi*, 1996; *Zanchi et al.*, 2006]. The Central Alborz form a ~100-km-wide asymmetric "V"-shaped structure, characterized by folds and faults trending WNW-ESE in the western part, and NE-SW in the eastern part [e.g., *Stöcklin*, 1968, 1974; *Berberian*, 1983; *Jackson et al.*, 2002; *Allen et al.*, 2003b; *Guest et al.*, 2006; *Nazari*, 2006; *Ritz et al.*, 2006; *Solaymani Azad et al.*, 2011b]. Damavand is located within a transition zone between the WNW-ESE and NE-SW structural trends, and reaches an altitude of 5670 m. Even though its base is resting on a ≥2500 m high plateau, the volcanic edifice itself is >3000 m-high.

4.2.1. Damavand Volcanism

[39] Damavand volcano results from the accumulation of >400 km^3 of trachyandesite lavas and subordinate pyroclastic material [*Allenbach*, 1966; *Mehdizadeh et al.*, 2002; *Davidson et al.*, 2004]. Conversely to Mt. Ararat, Damavand constitutes the only polygenetic volcano in Central Alborz, representing an isolated example of volcanism. The current cone (Young Damavand) rests upon an eroded apron of earlier deposits related to the eruption of the Old Damavand, slightly to the northeast, without evident compositional distinction [*Davidson et al.*, 2004]. The Young Damavand is NE-SW elongated with flattening f ~0.33 (see section 3). The same NE-SW trend is also highlighted by the alignment of the few parasitic vents (Figure 10) on the SW and NE flanks of the volcano [*Brousse and Moine Vaziri*, 1982; *Davidson et al.*, 2004; *Liotard et al.*, 2008], suggesting a focusing of volcanic activity along the NE-SW direction. This direction is coincident with the modern NE-SW compression in the Central and Eastern Alborz [e.g., *Tchalenko et al.*, 1974; *Zanchi et al.*, 2006; *Abbassi and Farbod*, 2009; *Javidfakhr et al.*, 2011a]. The earliest eruptions of Damavand began at ca. 1.8 Ma, when more mafic magmas were erupted. Then, up to 7 ka, a much larger volume of differentiated magma was erupted, indicating the emplacement of a stable storage system in the crust, allowing fractional crystallization and crustal assimilation [*Mehdizadeh et al.*, 2002; *Davidson et al.*, 2004].

[40] According to *Liotard et al.* [2008], the most primitive rocks are shoshonitic basalts (absarokites) (Figure 7a), characterized by high LILE/HFSE, high La/Yb, La/Nb (Figure 7b) and Th/Ta, low Sr and high Nd isotope ratios. Most of the products are intermediate rocks of a shoshonitic suite (banakites), with higher Sr and lower Nd isotope ratios compared to the mafic rocks. The geochemical modeling and the correlation of Sr, Nd and Pb isotope data with the differentiation degree indicate that the Damavand suite may derive from differentiation in crustal reservoirs by fractional crystallization and crustal assimilation, starting from mantle-derived parent magmas. The primary magmas may have originated by low degrees of partial melting of a metasomatized mantle source in which a K-bearing phase, possibly phlogopite, was present. The high Ba content and Ba/Nb suggest that metasomatism occurred by means of subduction-derived fluids carrying fluid-mobile elements. The high La/Yb is in agreement with a rather deep mantle source, in the garnet stability field. As regards the causes for Damavand primary magma genesis, given the post-collisional setting, *Liotard et al.* [2008] consider it unlikely that the fluids responsible for metasomatism of the mantle source induced partial melting. *Liotard et al.* [2008] link the metasomatic features to an older subduction, and relate the initiation of partial melting to the higher temperatures in the mantle following the suggested lithospheric delamination in the region [*Pearce et al.*, 1990; *Davidson et al.*, 2004; *Sodoudi et al.*, 2009]. Geochemical data also do not support a subduction-related magmatism [*Davidson et al.*, 2004], conversely to previous studies [*Aftabi and Atapour*, 2000]. Also, current subduction beneath the Damavand volcano is not supported by seismic data, and no surface expression of an associated trench or suture has been identified [see *Davidson et al.*, 2004]. *Mirnejad et al.* [2010] also argue against a role for subduction-related fluids and highlight the intraplate character of Damavand rocks on trace element discrimination diagrams. In their work, the Damavand products are alkali olivine basalts and trachyandesites, and their geochemical features are explained with low degrees of partial melting of an enriched mantle source, with slight upper crustal contamination accompanying differentiation processes in the crust. These authors, therefore, envisage a different, enriched, mantle source, but agree on the delamination of a thickened lithosphere being a probable cause for initiating partial melting.

[41] The delamination hypothesis to explain magmatism at Damavand is also supported by several geophysical data in Central Alborz; despite average elevations of 2000 m, the crustal thickness beneath Central Alborz is estimated at ~46–58 km [*Sodoudi et al.*, 2009; *Abbassi et al.*, 2010; *Radjaee et al.*, 2010]. Below Damavand, the larger crustal thickness, estimated at 55–68 km, is explained with the addition of magma at the base of the crust, with a relatively thin lithospheric mantle [*Sodoudi et al.*, 2009; *Shad Manaman et al.*, 2011]. The Alborz Mountains may have been previously over-thickened [*Dilek and Moores*, 1999],

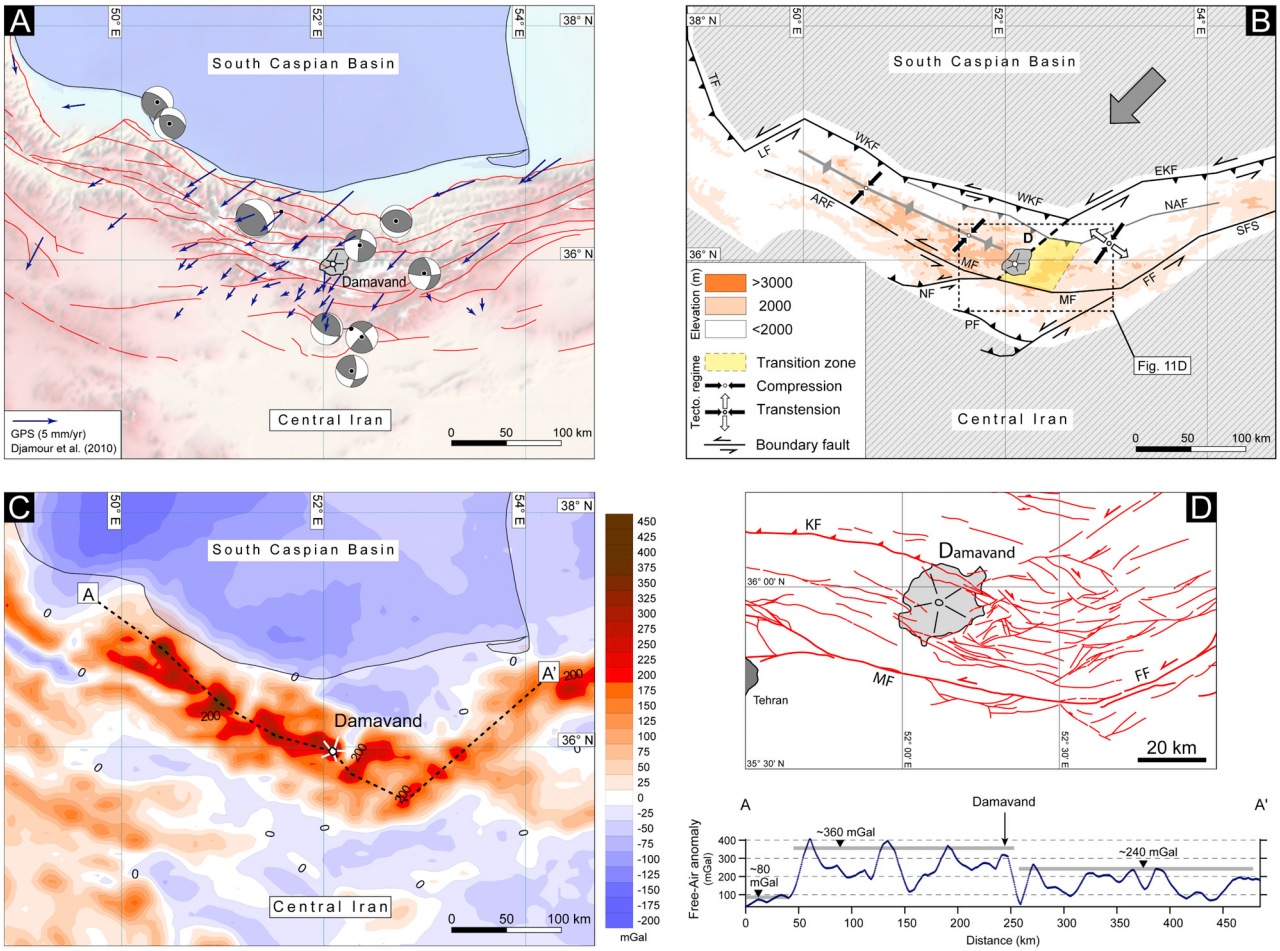

Figure 11. (a) Geologic, geodetic and seismologic data characterizing the present-day kinematics of Central Alborz. Faults are in red [after *Jackson et al.*, 2002; *Hessami et al.*, 2003]. Arrows are GPS velocity vectors (mm/yr) relative to Central Iran [after *Djamour et al.*, 2010]. Earthquakes focal mechanisms (beach balls) are from Harvard catalog (http://www.globalcmt.org/CMTsearch.html), while epicenters are from the ISC–EHB Bulletin (International Seismic Centre, Thatcham, United Kingdom, 2009, http://www.isc.ac.uk). (b) Idealized tectonic model for the present-day deformation in Central Alborz. Both geometry and kinematics of tectonic structures and topography in Central Alborz result from the relative motion (gray arrow) between Central Iran and south Caspian blocks (cross-hatched parts). As a part of SW motion of the South Caspian Basin-Central Iran may be accommodated by the North Alborz Fault (NAF), a transition zone occurs between the western compressional and eastern transtensional tectonic domains. Abbreviations refer to faults: ARF, Alamut-Rud; EKF, East Khazar; FF, Firuzkuh; LF, Lahijan; MF, Mosha; NF, North Tehran; PF, Parchin; SFS, Shahrud system; TF, Talesh; WKF, West Khazar. (c) Free-air gravity anomaly (available at http://bgi.omp.obs-mip.fr/index.php/eng/Data-Products) for Central Alborz and adjacent regions (South Caspian Basin is interpolated). Dashed line shows location of A–A′ profile (below the map) on which the mean value for peaks in free-air gravity anomaly is shown by gray lines. Damavand lies at the boundary between two distinct domains. (d) Detailed fault map [after *Haghipour et al.*, 1986; *Vahdati Daneshmand*, 1991; *Aghanabati and Hamedi*, 1994; this study] indicating structural transition between the western and eastern portions of Central Alborz, where the Damavand volcano is located. KF is Kandavan Fault.

but are now largely underlain by anomalously low-density upper mantle and a hot and weak lower crust and mantle [*Toksöz and Bird*, 1977; *Kadinsky-Cade et al.*, 1981; *Guest et al.*, 2007]. Also, an inefficient Sn wave propagation, a high attenuation and a low Q have been highlighted below Central Alborz, similarly to NW and NE Iran [*Kadinsky-Cade et al.*, 1981; *Rodgers et al.*, 1997; *Rahimi et al.*, 2010]. Finally, the Central Alborz underwent significant uplift (~10 km) in the last 5 Ma, from the onset of continental collision [*Axen et al.*, 2001; *Allen et al.*, 2002], even though the collision may have initiated at 12 Ma [*Guest et al.*, 2006].

4.2.2. Tectonic Setting of Damavand

[42] Despite the possibility that lithospheric delamination may have generated the magma below Damavand, the

definition of the structural setting controlling the rise and extrusion of magma from Damavand is more debated. Here we propose an original working hypothesis of the tectonic setting of Damavand, based on all available data.

[43] According to geological [e.g., *Allen et al.*, 2003b; *Ritz et al.*, 2006; *Nazari*, 2006] and seismological studies [e.g., *Jackson et al.*, 2002; *Tatar et al.*, 2007; *Tatar and Hatzfeld*, 2009], the present-day deformation in Alborz appears partitioned along range-parallel thrusts and left-lateral faults. However, the interaction between the asymmetric "V" shape structure of Central Alborz and the rotational motion of the South Caspian Basin relative to Eurasia produces a more complex velocity field [*Djamour et al.*, 2010]. At the southern side of the Alborz, left-lateral faulting is well documented by focal mechanisms of earthquakes within both the western part, along WNW-striking faults, such as the Mosha Fault [e.g., *Hedayati et al.*, 1976; *Jackson et al.*, 2002; *Ashtari et al.*, 2005], and the eastern part of Central Alborz along NE-striking Firuzkuh and Astaneh faults [*Nemati et al.*, 2011] (Figure 11a). This left-lateral kinematics is also supported by tectonic geomorphology [e.g., *Trifonov et al.*, 1996; *Allen et al.*, 2003b; *Hessami et al.*, 2003; *Ritz et al.*, 2003; *Solaymani et al.*, 2003; *Bachmanov et al.*, 2004; *Solaymani Azad et al.*, 2011b] and InSAR [*Shirzaei et al.*, 2011] investigations carried out along the Mosha Fault, Taleghan and Firuzkuh faults [*Nazari*, 2006; *Nazari et al.*, 2009], and the Shahrud fault system comprising the Astaneh Fault [*Hollingsworth et al.*, 2010; *Javidfakhr et al.*, 2011b] (Figure 11b). At the northern side, the southwest- to southeast-dipping Khazar Fault forms the boundary between Central Alborz and the South Caspian Basin [e.g., *Berberian*, 1983; *Tatar et al.*, 2007]. The fault follows the V shape pattern of the northern flank of Central Alborz, with a complex kinematics [e.g., *Allen et al.*, 2003b; *Guest et al.*, 2006; *Nazari*, 2006]. Seismological evidence [*Tatar et al.*, 2007] suggests that, in the western part, the Khazar Fault is the source of the 2004 Baladeh thrust faulting earthquake, and it is at least 35 km deep.

[44] The analysis of a dense network of GPS sites covering Central Alborz [*Djamour et al.*, 2010] has revealed important kinematic aspects of the present-day deformation. For the faults south of the range (Mosha, Firuzkuh, and Astaneh), the vertical component of faulting is not significant, consistently with the fact that the faults are mainly left-lateral. Conversely, the Khazar Fault is divided into two distinct portions: (1) the western segment is mainly a thrust fault (Figures 11a and 11b) slipping at ~6 mm/yr, with a left-lateral component of ~2–3 mm/yr; (2) the eastern segment (Figures 11a and 11b) is predominately left-lateral (~5 mm/yr) accompanied with a lesser component of thrust faulting at ~2–3 mm/yr. The obliquity of the South Caspian Block relative to Central Iran varies from ~25° in the western part of Central Alborz to ~70° in the eastern part of the range [*Djamour et al.*, 2010] (Figures 11a and 11b).

[45] All these observations imply that the eastern part of Central Alborz principally accommodates strike-slip deformation, while the western part of Central Alborz takes up compressional deformation by thrust faulting and shortening (Figures 11a and 11b). Such a deformation pattern sums up almost all the geological and seismological observations mentioned above, and may explain some other features of the range. For instance, maximum topography of the range is concentrated in the western part between the compressional segment of the Khazar Fault and the strike-slip Mosha Fault (Figure 11b). An abrupt ~500 m topographic contrast is observed between the western parts of Central Alborz, with a mean altitude of 3500 m, and the eastern part, with a mean altitude of 3000 m. A similar pattern is also supported by free-air gravity data (Figure 11c); the western part of Alborz shows a free-air gravity anomaly of ~360 mGal, while only minor areas in the eastern part exceed an anomaly of ~240 mGal. Interestingly, the boundary for the variation in topography and free-air gravity anomalies is NE-SW oriented along the southwestward extrapolation of the eastern segment of the Khazar Fault (Figure 11b). This suggests that the topography of central Alborz reflects kinematics and geometry of its structure (Figure 11d), in close interaction with lithospheric adjustment. In fact, free-air gravity suggests that the elevation of Alborz is largely supported by the elastic strength of the Iranian and/or the South Caspian blocks [*Radjaee et al.*, 2010]. However, it appears that the more compressed WNW-trending portion of the belt is more affected by such a process; with the Alborz range overthrusting the surrounding rigid blocks (Figure 11b). For Damavand volcano, lithospheric delamination has been proposed as the main cause originating magma production [e.g., *Davidson et al.*, 2004; *Liotard et al.*, 2008]. If delamination has occurred, it is expected that the most compressed and uplifted area in Central Alborz may also correspond with the area where a dense mass has been removed at the base of the lithosphere, consistently with what observed elsewhere [*Gioncada et al.*, 2010, and references therein]. Under these assumptions, Damavand may lie in the easternmost part of the delaminated portion of the range (Figure 11). As reported above, Damavand is located at the junction between two distinct (eastern and western) tectonic domains (Figures 11a, 11b, and 11d). At this boundary, predominant shortening in the western transpressional regime [e.g., *Tatar et al.*, 2007; *Djamour et al.*, 2010] turns into an eastern transtensional regime, with NE-trending left-lateral faulting [e.g., *Jackson et al.*, 2002; *Nazari*, 2006; *Nemati et al.*, 2011]. The boundary between the two domains is parallel to the regional NE-SW $\sigma 1$ stress axis [*Abbassi and Shabanian*, 1999; *Abbassi et al.*, 2003; *Zanchi et al.*, 2006; *Abbassi and Farbod*, 2009; *Javidfakhr et al.*, 2011a] and to the relative block motion between the South Caspian Basin and Central Iran [*Djamour et al.*, 2010]. Moreover, along this boundary, the more extended eastern part is juxtaposed against the more compressed western part (Figure 11b). This boundary is expected to experience a significant stress gradient, due to an "edge effect," induced by the lower confinement of the crust toward the east. These differential buttressing conditions may induce local extension in the crust, enhancing the emplacement of magma along major crustal fractures below Damavand.

[46] It is thus proposed that the particular location of Damavand, an isolated stratovolcano within a fold and thrust belt, may be related to a combination of melt availability due to delamination of the lithosphere below the shortened area (Figures 11b and 11c), as well as suitable structural conditions in the crust, provided by the stress gradient (Figures 11b

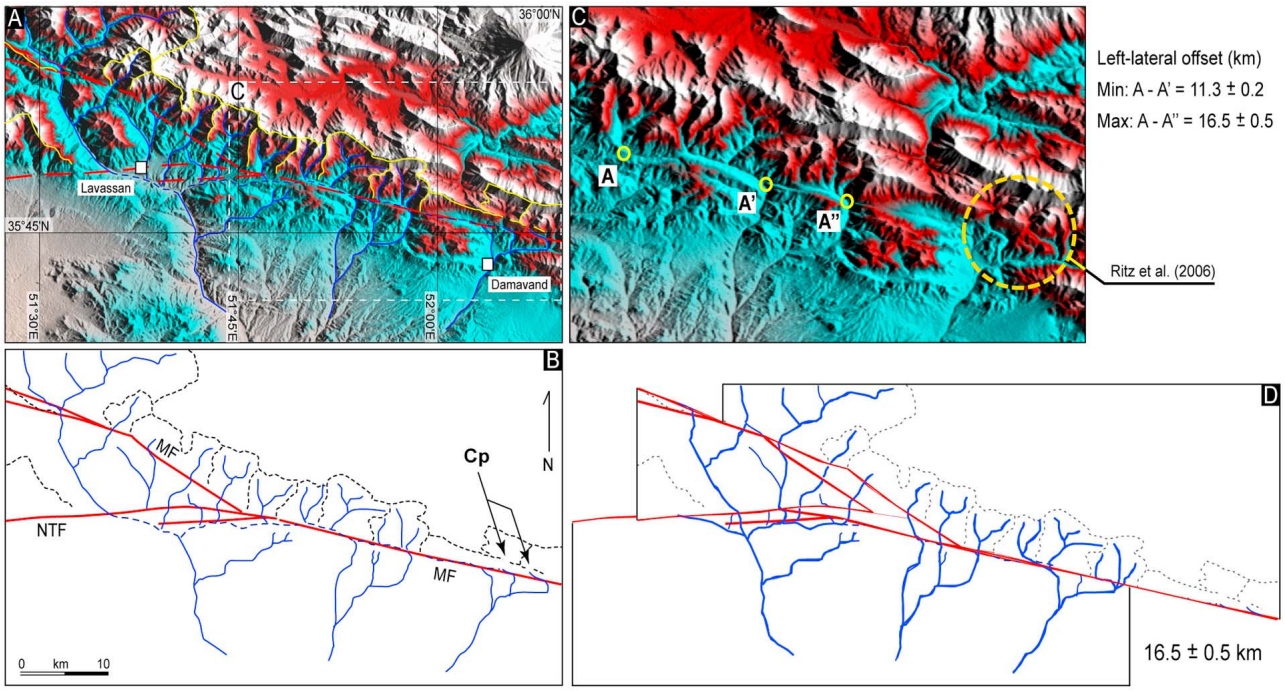

Figure 12. (a) Shaded relief image (SRTM digital topographic data) of the eastern portion of the Mosha Fault showing streams (blue line) and their associated drainage basins (yellow line) offset along the fault (red line). The peak in the upper right is Damavand volcano. (b) Morphotectonic interpretation of Figure 12a. Both streams and drainage basins are asymmetrically distributed on either sides of the Mosha Fault, with an overall left-lateral offset. The easternmost stream set does not correspond to the elongated catchment area just north of the fault. The two eastern streams have incised in the northern watershed of the catchment area, capturing parts of drainage basins on the other side of the watershed. (c) A-A′ and A-A″ are piercing points along the Mosha Fault, which represent minimum and maximum geomorphic offsets of ∼11 and ∼16 km, respectively. The piercing point A indicates the outlet of a catchment area (beheaded stream) that has not any counterpart inlet before A′, implying that the total geomorphic offset along the fault is at least ∼11 km. Drainage offsets reported by *Ritz et al.* [2006] is marked by dashed circle. (d) Geomorphic reconstruction of drainage systems displaced by the Mosha Fault, indicating a total geomorphic offset of ∼16 km.

and 11d). Along the Alborz range, such a combination of tectono-magmatic lithospheric processes is apparently met only in the Damavand area, and may therefore explain its location and significant magmatic production.

4.2.3. Onset of the Present-Day Kinematics in Central Alborz

[47] The onset of the present-day kinematics of the South Caspian Basin is debated [e.g., *Axen et al.*, 2001; *Jackson et al.*, 2002; *Allen et al.*, 2003a; *Ritz et al.*, 2006; *Ballato et al.*, 2008; *Solaymani Azad et al.*, 2011b] as it varies between ∼5 Ma [e.g., *Axen et al.*, 2001; *Allen et al.*, 2003a] and 1.5 Ma [*Ritz et al.*, 2006; *Solaymani Azad et al.*, 2011b]. The upper bound relies on the assumption that the ∼3 km total left-lateral offset along the Mosha Fault has been achieved by cumulative displacements at a constant Holocene slip rate of ∼2.2 mm/yr. But, these ∼3 km of left-lateral geomorphic offset have been recorded by streams deflected within the Mosha fault zone (Figure 12) [*Ritz et al.*, 2006; *Solaymani Azad et al.*, 2011b] and are far from being representative of the total left-lateral offset of the fault. Previously, a maximum geological offset of 30–35 km was proposed by *Allen et al.* [2003b] comparing two counterparts of a deformed anticline cut by the Mosha Fault. But, neither geometry, nor structure of the fold can be reconstructed by the restoration of 30–35 km left-lateral offset, indicating that the present geometry of the anticline may imply a complex faulting history of the Mosha Fault [e.g., *Guest et al.*, 2006; *Moinabadi and Yassaghi*, 2007; *Yassaghi and Madanipour*, 2008].

[48] Our original geomorphic reconstruction of the main-streams left-laterally offset along the Mosha Fault, between the town of Damavand (not to be confused with the volcano, to the north) and Lavassan (Figure 12), reveals total geomorphic offsets of 11.3 ± 0.2 and 16.5 ± 0.5 km, as the respective lower and upper limits for the cumulative left-lateral offset of the fault (Figures 12c and 12d). For the minimum offset of 11.3 ± 0.2 km, the westernmost beheaded stream on the north side of the fault is related to the nearest stream in the east, on the south side (Figure 12c). But, the restoration of 16.5 ± 0.5 km of maximum left-lateral offset allows us to properly reconstruct three drainage systems that have been offset along the fault (Figure 12d). Assuming a

temporally constant slip rate on the Mosha Fault, the application of ~2.2 mm/yr Holocene slip rate [*Ritz et al.*, 2006] to both the 11.3 ± 0.2 and 16.5 ± 0.5 km geomorphic offsets yields onset ages of between ≤7 and ≥5 Ma for left-lateral faulting along the Mosha Fault. This age estimate seems consistent with the age proposed by *Guest et al.* [2006] for the initiation of left-lateral faulting along the WNW-striking faults, including the Mosha Fault. This age consistency suggests that the present-day tectonic configuration in the Alborz Mountains, in relation with the South Caspian Basin tectonics (under-thrusting and subduction), has been established not later than 5 Ma [e.g., *Axen et al.*, 2001; *Allen et al.*, 2003a, 2004].

5. Discussion

5.1. Interpretation of the Sar'akhor Data

[49] The structural data collected in the Meshkan triangle suggest that this area underwent significant strike-slip faulting during Neogene. A NW-trending compression, probably active until Late Pliocene (~2.4 Ma), was responsible for dextral faulting on the WSW-striking Farhadan Fault, on the northern side of the triangle, and for sinistral faulting on the Chakaneh Fault, on the eastern side of the triangle (Figure 6) [*Shabanian et al.*, 2010]. The combined motion of both faults would have allowed the SW extrusion of the wedge within, extending the junction area between the two faults, where Sar'akhor volcano is located (Figure 6). The fact that the Miocene–Late Pliocene volcanic activity at Sar'akhor was coeval with such a tectonic scenario suggests that the two strike-slip faults in this period where creating the structural conditions to enhance the rise, emplacement and extrusion of magma through the crust. Therefore, during Miocene – Late Pliocene, strike-slip faulting allowed the development of areas of localized extension, controlling shallow magmatism and the development of a stratovolcano with a significant size (~3.5 km-high; Figures 8 and 9) and productivity.

[50] There is widespread evidence of strike-slip faults controlling volcanism [e.g., *Tibaldi*, 1992; *Bellier and Sébrier*, 1994; *Lécuyer et al.*, 1997; *Bellier et al.*, 1999; *Lavenu and Cembrano*, 1999; *Riller et al.*, 2001; *García Palomo et al.*, 2004; *Acocella and Funiciello*, 2010, and references therein] or the syntectonic emplacement of plutons, constituting the magma chambers of arc volcanoes [e.g., *Morand*, 1992; *Moreau et al.*, 1994; *Vigneresse*, 1995; *Castro and Fernandez*, 1998; *Gibbons and Moreno*, 2002; *Wagner et al.*, 2006]. However, this evidence refers to a common mechanism to create extension in strike-slip settings, through the development of pull-apart like structures, releasing bends or tension gashes along a principal displacement zone. Our study shows a different mechanism responsible for extension, and thus the enhancement of volcanism in strike-slip settings, related to the extrusion of a wedge laterally bordered by strike-slip faults (Figure 13b). Such a mechanism is capable of inducing a localized decompression (extension) at its rear, as well as to produce the space required for the intrusion of magma in the crust, enhancing the development of shallow magmatic reservoirs feeding volcanism (Figure 6). To our knowledge, this is the first example of volcanism-enhanced block extrusion, thus constituting a new model illustrating volcano-tectonic relationships.

[51] From Late Pliocene (≥2.4 Ma), the stress conditions changed, and the modern NE-trending compression [*Shabanian et al.*, 2010] inverted the strike-slip motion of the Farhadan and Chakaneh faults (section 3.1.3). This has caused northeast movement of the Meshkan triangle, inducing the compression in the junction area between the two faults. There is no evidence that volcanic activity in the Meshkan area continued after Late Pliocene. The end of volcanism may imply a correlation with the new structural setting. However, such a possibility needs to be confirmed, as it also depends from the generation and availability of magma at depth. It has been shown that a compressive setting may not hinder volcanism, provided that magma is available at depth [*Tibaldi*, 2005; *Galland et al.*, 2007; *Acocella et al.*, 2008; this study].

5.2. Relationships With Nearby Current Analogues

[52] Placing the Sar'akhor case into a wider context allows a better definition of how intraplate collisional volcanoes work. Current analogues of Sar'akhor in the East Anatolian-Iranian plateaus are Damavand and Ararat volcanoes. Even though the composition of the latter two volcanoes is slightly more mafic, their overall features can be considered as similar to Sar'akhor, the ~3 km-high polygenetic edifice located within the same collision zone (Table 2). The tectono-magmatic constraints considered in this study have been summarized in Figure 13, which is meant to be representative of all the shallower and deeper conditions met in Sar'akhor, Ararat and Damavand volcanoes.

[53] At depth, magma generation and availability is provided by the rise of asthenosphere, probably due to slab break-off or lithospheric delamination (Table 2). Both processes are expected to be representative, even though not exclusive, of the deep evolution of a mature collisional zone. As a matter of fact, intraplate collisional magmatism associated with mantle delamination or slab break-off has been repeatedly inferred in the Central Andes, enhanced by transtensional structures at upper crustal levels [*Riller et al.*, 2001; *Gioncada et al.*, 2010; *Acocella et al.*, 2011, and references therein], and in the Basin and Range and Western Canada [*Ducea*, 2011, and references therein].

[54] In the crust, local extension enhancing volcanism may be induced by (1) strike-slip faults creating an extruding wedge (Figure 13a; Sar'akhor), (2) strike-slip faults creating releasing relay zones and pull-apart structures (Figure 13b; Ararat) [*Karakhanian et al.*, 2002, 2004], or (3) the coexistence of transpressional and transtensional domains producing a sharp stress gradient (Figure 13c; Damavand) (Table 2). Even though these examples show three different mechanisms of structural control on volcanism, in the three cases strike-slip faults play the principal role in creating zones of localized extension to enhance and accommodate magma rise in the crust. This confirms that, within collisional settings, strike-slip tectonics may be the most effective means to provoke the rise and extrusion of magma from volcanoes. This fact is in close agreement with previous studies [e.g., *Acocella and Funiciello*, 2010, and references therein], showing that the magmatic productivity of volcanic arcs in oblique convergence settings characterized by deep-seated strike-slip faults is significant.

[55] The possibilities illustrated in Figure 13 reflect the state of the art of our knowledge at the surface and at depth

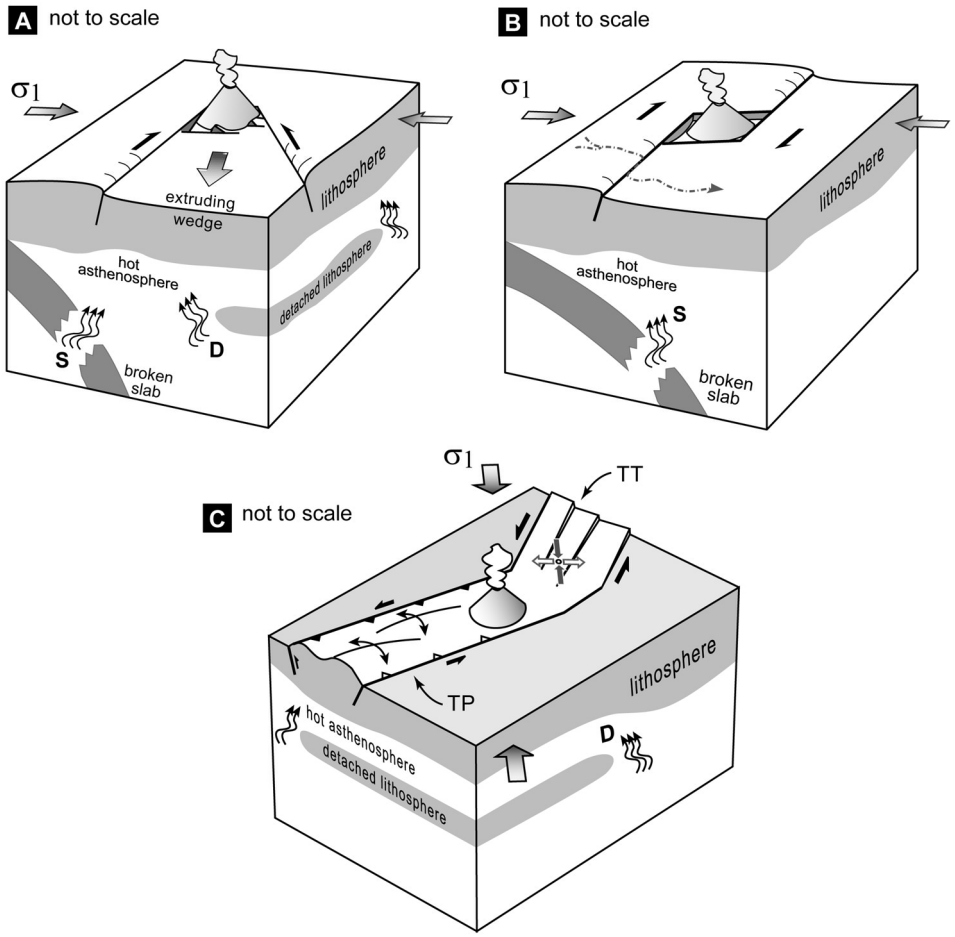

Figure 13. Simplified models summarizing the possible tectonic control on intraplate magmatism in collisional settings, both at depth (slab break-off or delamination) and at the surface (three types of transtensional structures). (a) Wedge extrusion derived from Sar'akhor. (b) Local extension in a releasing relay zone/pull-apart structure (Ararat). (c) Stress gradient within an orogen (Damavand); TT, Transtension; TP, transpression. See text for details. Letters D and S indicate asthenosphere rise due to lithospheric delamination and slab beak-off, respectively.

in three polygenetic intraplate volcanoes in a similar collisional setting. These are not meant to provide a comprehensive review of all the possible conditions controlling volcanism in any intraplate setting. It is expectable that, studying more in detail other intraplate volcanoes, additional mechanisms controlling the generation and the rise of magma will be proposed. So far, our limited knowledge allows highlighting the importance of post collisional rise of

Table 2. Summary of Original and Previous Constraints on the Tectonic and Magmatic Features of the Three Volcanoes Compared in This Study (References in the Related Text)

Volcano	Sar'akhor	Damavand	Ararat
Height (km)	3.0 ± 0.9	~2.9	~3.8
Composition	Andesites, dacites (adakites)	Alkali basalts, trachyandesites	Trachybasalts, andesites
Structural setting	Transtensional	Transpressional/Transtensional	Transtensional
Tectonic mechanism	Wedge extrusion	Stress Gradient	Pull-Apart
Activity	Miocene – Late Pliocene	Quaternary	Quaternary
Oceanic subduction end	Late Paleocene	No subduction	Late Middle Miocene
Source rock composition	Basalt, metamorphosed in eclogite facies	Garnet and phlogopite-rich lherzolite	Spinel lherzolite
Sources rocks	Slab or lower crust melting, possible crustal contamination	Mantle melting	Mantle melting
Scenario for magma generation	Oceanic slab break-off or intra-mantle delamination	Delamination of lower mantle lithosphere	Oceanic/continental slab break-off (?)

the asthenosphere in generating magma, as well as the significance of strike-slip, especially transtensional tectonics at crustal and even perhaps at lithospheric scales in allowing the rise of magma.

6. Conclusions

[56] Original and preexisting data allow us to reconstruct the tectono-magmatic features of the Miocene–Late Pliocene Sar'akhor volcano, northeast Iran. NW-oriented compression activated ~E-W dextral faults to the northwest of Sar'akhor and N-S sinistral faults to the southeast, creating an extruding wedge in the location of volcano. Such a mechanism has never been proposed before to control volcanic activity. The adakitic composition of the volcano is compatible with magma generation through post collisional processes of either oceanic slab or continental lower crust melting, which in turn, are triggered by asthenospheric rise after detachment of the slab or intramantle delamination, respectively.

[57] Two independent reconstructions suggest that Sar'akhor was an important volcanic edifice, 3.0 ± 0.9 km high. Available data from current analogues Damavand and Ararat volcanic edifices, with nearly similar size, suggest magma generation due to rising of hot asthenosphere following lithospheric delamination (Damavand) or slab break-off (Ararat). The rise, emplacement and extrusion of magma occurred in transtensional tectonic settings or in the transition between adjacent transpressional and transtensional domains.

[58] The features common to Sar'akhor, Damavand and Ararat allow proposing a general, though not exhaustive, model that highlights the significance of crustal transtensional structures in allowing the rise and extrusion of magma.

[59] **Acknowledgments.** This study was carried under the frame of a cooperation program between CEREGE and Roma Tre, while V.A. was visiting professor at CEREGE. Field surveys in the Meshkan area (2006–2007) were funded by the INSU-CNRS (Dyeti and PNRN programs, France), French Ministry of Research (ACI FNS program), and the International Institute of Earthquake Engineering and Seismology (IIEES, Iran), supervised by D. Hatzfeld and M. Ghafouri Ashtiani. V. Grimault, C. Duhamel, and the staff of the SCAC of the French Embassy in Tehran are acknowledged for their support. C. Faccenna provided initial encouragement. M. Shirzaei provided helpful discussions. We are grateful to F. Chalot-Prat, an anonymous reviewer, and C. Doglioni (Associate Editor) for helpful and constructive reviews. The editor Onno Oncken is acknowledged for help and handling the manuscript. J.-J. Cochemé and M. R. Abbassi are acknowledged for the petrographic analysis of dacitic samples and field assistance in the Meshkan area, respectively.

References

Abbassi, M. R., and Y. Farbod (2009), Faulting and folding in Quaternary deposits of Tehran's piedmont (Iran), *J. Asian Earth Sci.*, *34*, 522–531, doi:10.1016/j.jseaes.2008.08.001.

Abbassi, M. R., and E. Shabanian (1999), Evolution of the Stress Field in Tehran Region during the Quaternary, paper presented at 3th International Conference on Seismology and Earthquake Engineering, Int. Inst. of Earthquake Eng. and Seismol., Tehran.

Abbassi, M. R., E. Shabanian, Y. Farbod, K. Feghhi, and H. Tabassi (2003), The state of contemporary stress in the southern flank of central Alborz [in Persian with English abstract], *Rep. 81-2003-7*, Int. Inst. of Earthquake Eng. and Seismol., Tehran.

Abbassi, A., A. Nasrabadi, M. Tatar, F. Yaminifard, M. Abbassi, D. Hatzfeld, and K. Priestley (2010), Crustal velocity structure in the southern edge of the Central Alborz (Iran), *J. Geodyn.*, *49*, 68–78, doi:10.1016/j.jog.2009.09.044.

Acocella, V., and F. Funiciello (2010), Structural control of arc volcanism and related kinematic setting: An overview, *Earth Planet. Sci. Lett.*, *289*, 43–53, doi:10.1016/j.epsl.2009.10.027.

Acocella, V., T. Yoshida, R. Yamada, and F. Funiciello (2008), Structural control on Late Miocene to Quaternary volcanism in the NE Honshu arc, Japan, *Tectonics*, *27*, TC5008, doi:10.1029/2008TC002296.

Acocella, V., A. Gioncada, R. Omarini, U. Riller, R. Mazzuoli, and L. Vezzoli (2011), Tectono-magmatic characteristics of the eastern Calama-Olacapato-El Toro lineament, Central Andes, *Tectonics*, *30*, TC3005, doi:10.1029/2010TC002854.

Afshar Harb, A. (1979), The stratigraphy, tectonics and petroleum geology of the Kopet Dagh region, northeastern Iran, PhD thesis, Pet. Geol. Sect., R. School of Mines, Imp. Coll. of Sci. and Technol., London.

Aftabi, A., and H. Atapour (2000), Regional aspects of shoshonitic volcanism in Iran, *Episodes*, *23*, 119–125.

Agard, P., J. Omrani, L. Jolivet, and F. Mouthereau (2005), Convergence history across Zagros (Iran): Constraints from collisional and earlier deformation, *Int. J. Earth Sci.*, *94*, 401–419, doi:10.1007/s00531-005-0481-4.

Aghanabati, A., and A. R. Hamedi (1994), Geological map of Iran, Semnan sheet, *Map G5*, scale 1:250 000, Geol. Surv. of Iran, Tehran.

Ahmadzadeh, G., A. Jahangiri, D. Lentz, and M. Mojtahedi (2010), Petrogenesis of Plio-Quaternary post-collisional ultrapotassic volcanism in NW of Marand, NW Iran, *J. Asian Earth Sci.*, *39*(1–2), 37–50, doi:10.1016/j.jseaes.2010.02.008.

Alavi, M. (1992), Thrust tectonics of the Binalood region, NE Iran, *Tectonics*, *11*, 360–370, doi:10.1029/91TC02217.

Alavi, M. (1996), Tectonostratigraphic synthesis and structural style of the Alborz mountain system in northern Iran, *J. Geodyn.*, *21*, 1–33, doi:10.1016/0264-3707(95)00009-7.

Alberti, A., P. Comin-Chiaramonti, S. Sinigoi, M. Nicoletti, and C. Petrucciani (1980), Neogene and Quaternary volcanism in Eastern Azerbaijan (Iran): Some K-Ar age determinations and geodynamics implications, *Geol. Rundsch.*, *69*, 216–225, doi:10.1007/BF01869034.

Al-Lazki, A. I., D. Seber, E. Sandvol, N. Turkelli, R. Mohamad, and M. Barazangi (2003), Tomographic Pn velocity and anisotropy structure beneath the Anatolian plateau (eastern Turkey) and the surrounding regions, *Geophys. Res. Lett.*, *30*(24), 8043, doi:10.1029/2003GL017391.

Al-Lazki, A. I., E. Sandvol, D. Seber, M. Barazangi, N. Turkelli, and R. Mohamad (2004), Pn tomographic imaging of mantle lid velocity and anisotropy at the junction of the Arabian, Eurasian, and African plates, *Geophys. J. Int.*, *158*, 1024–1040, doi:10.1111/j.1365-246X.2004.02355.x.

Allen, M. B., S. Jones, A. Ismail-Zadeh, M. Simmons, and L. Anderson (2002), Onset of subduction as the cause of rapid Pliocene-Quaternary subsidence in the South Caspian Basin, *Geology*, *30*(9), 775–778, doi:10.1130/0091-7613(2002)030<0775:OOSATC>2.0.CO;2.

Allen, M. B., S. J. Vincent, I. Alsop, A. Ismail-zadeh, and R. Flecker (2003a), Late Cenozoic deformation in the South Caspian region: Effects of a rigid basement block within a collision zone, *Tectonophysics*, *366*, 223–239, doi:10.1016/S0040-1951(03)00098-2.

Allen, M. B., M. R. Ghassemi, M. Shahrabi, and M. Qorashi (2003b), Accommodation of late Cenozoic oblique shortening in the Alborz range, northern Iran, *J. Struct. Geol.*, *25*, 659–672, doi:10.1016/S0191-8141(02)00064-0.

Allen, M., J. Jackson, and R. Walker (2004), Late Cenozoic reorganization of the Arabia-Eurasia collision and the comparison of short-term and long-term deformation rates, *Tectonics*, *23*, TC2008, doi:10.1029/2003TC001530.

Allenbach, P. (1966), Geologie und petrographie des Damavand und seiner Umgebung (Zentral Elburz): Iran [in German], *Mitt. Geol. Inst. Eidg. Tech. Hochsch. Univ. Zurich*, *63*, 1–145.

Amini, B., and N. H. Khan-Nazer (2000), Geological map of Iran, Mashkan sheet, *Map Ser. 7563*, scale 1:100 000, Geol. Surv. of Iran, Tehran.

Anderson, D. L., and K. A. Schramm (2005), Global hotspot maps, in *Plates, Plumes, and Paradigms*, edited by G. R. Foulger et al., *Spec. Pap. Geol. Soc. Am.*, *388*, 19–29, doi:10.1130/0-8137-2388-4.19.

Angus, D. A., D. C. Wilson, E. Sandvol, and J. F. Ni (2006), Lithospheric structure of the Arabian and Eurasian collision zone in eastern Turkey from S-wave receiver functions, *Geophys. J. Int.*, *166*, 1335–1346, doi:10.1111/j.1365-246X.2006.03070.x.

Ashtari, M., D. Hatzfeld, and M. Kamalian (2005), Microseismicity in the region of Tehran, *Tectonophysics*, *395*, 193–208, doi:10.1016/j.tecto.2004.09.011.

Authemayou, C., D. Chardon, O. Bellier, Z. Malekzadeh, E. Shabanian, and M. R. Abbassi (2006), Late Cenozoic partitioning of oblique plate convergence in the Zagros fold-and-thrust belt (Iran), *Tectonics*, *25*, TC3002, doi:10.1029/2005TC001860.

Axen, G. J., P. J. Lam, M. Grove, D. F. Stockli, and J. Hassanzadeh (2001), Exhumation of thewestcentral Alborz mountains, Iran, Caspian subsidence,

and collision-related tectonics, *Geology*, *29*, 559–562, doi:10.1130/0091-7613(2001)029<0559:EOTWCA>2.0.CO;2.

Azizi, H., and H. Moinevaziri (2009), Review for tectonic setting for Cretaceous to Quaternary volcanism in NW Iran, *J. Geodyn.*, *47*, 167–179, doi:10.1016/j.jog.2008.12.002.

Bachmanov, D. M., V. G. Trifonov, K. Hessami, A. I. Kozhurin, T. P. Ivanova, E. A. Rogozhin, M. C. Hademi, and F. H. Jamali (2004), Active faults in the Zagros and central Iran, *Tectonophysics*, *380*, 221–241, doi:10.1016/j.tecto.2003.09.021.

Ballato, P., N. R. Nowaczyk, A. Landgraf, M. R. Strecker, A. Friedrich, and S. H. Tabatabaei (2008), Tectonic control on sedimentary facies pattern and sediment accumulation rates in the Miocene foreland basin of the southern Alborz mountains, northern Iran, *Tectonics*, *27*, TC6001, doi:10.1029/2008TC002278.

Barberi, F., L. Civetta, and J. Varet (1980), Sr Isotopic composition of Afar volcanics and its implication for mantle evolution, *Earth Planet. Sci. Lett.*, *50*, 247–259, doi:10.1016/0012-821X(80)90136-3.

Bauman A., O. Spies, and G. Lensch (1983), Strontium isotopic composition of post-ophiolitic Tertiary volcanics between Kashmar, Sabzevar and Quchan/NE Iran, in *Geodynamic Project (Geotraverse) in Iran*, *Rep. 51*, pp. 267–276, Geol. Surv. of Iran, Tehran.

Bellier, O., and M. Sébrier (1994), Relationship between tectonism and volcanism along the Great Sumatran fault zone deduced by Spot image analyses, *Tectonophysics*, *233*, 215–231, doi:10.1016/0040-1951(94)90242-9.

Bellier, O., H. Bellon, M. Sébrier, Sutanto, and R. C. Maury (1999), K-Ar age of the Ranau tuffs: Implications for the Ranau caldera emplacement and slip-partitioning in Sumatra (Indonesia), *Tectonophysics*, *312*, 347–359, doi:10.1016/S0040-1951(99)00198-5.

Berberian, M. (1983), The southern Caspian: A compressional depression floored by a trapped, modified oceanic crust, *Can. J. Earth Sci.*, *20*, 163–183, doi:10.1139/e83-015.

Berberian, M., and S. Arshadi (1976), On the evidence of the youngest activity of the North Tabriz Fault and the seismicity of Tabriz city, *Geol. Surv. Iran*, *39*, 397–418.

Berberian, F., and M. Berberian (1981), Tectono-plutonic episodes in Iran, in *Zagros, Hindu Kush, Himalaya: Geodynamic Evolution*, *Geodyn. Ser*, vol. 3, edited by H. K. Gupta and F. M. Delany, pp. 5–32, AGU, Washington, D. C., doi:10.1029/GD003p0005.

Berberian, M., and G. C. P. King (1981), Towards a paleogeography and tectonic evolution of Iran, *Can. J. Earth Sci.*, *18*, 210–265, doi:10.1139/e81-019.

Berberian, M., and R. S. Yeats (1999), Patterns of historical earthquake rupture in the Iranian plateau, *Bull. Seismol. Soc. Am.*, *89*, 120–139.

Berberian, F., I. D. Muir, R. J. Pankhurst, and M. Berberian (1982), Late Cretaceous and early Miocene Andean type plutonic activity in northern Makran and central Iran, *J. Geol. Soc.*, *139*, 605–614, doi:10.1144/gsjgs.139.5.0605.

Bina, M. M., I. Bucur, M. Pervot, Y. Meyerfeld, L. Daly, J. M. Cantagrel, and J. Mergoil (1986), Palaeomagnetism petrology and geochronology of Tertiary magmatic and sedimentary units from Iran, *Tectonophysics*, *121*, 303–329, doi:10.1016/0040-1951(86)90050-8.

Blundy, J., K. V. Cashman, and K. Berlo (2008), Evolving magma storage conditions beneath Mount St. Helens inferred from chemical variations in melt inclusions from the 1980–1986 and current (2004–2006) eruptions, *U.S. Geol. Surv. Prof. Pap.*, *1750*, 755–790.

Bosworth, W., and M. R. Strecker (1997), Stress field changes in the Afro-Arabian Rift System during the Miocene to recent period, in *Structure and Dynamic Processes in the Lithosphere of the Afro-Arabian Rift System*, edited by K. Fuchs et al., *Tectonophysics*, *278*, 47–62, doi:10.1016/S0040-1951(97)00094-2.

Bosworth, W., K. Burke, and M. Strecker (2003), Effect of stress fields on magma chamber stability and the formation of collapse calderas, *Tectonics*, *22*(4), 1042, doi:10.1029/2002TC001369.

Bozkurt, E. (2001), Neotectonics of Turkey–A synthesis, *Geodin. Acta*, *14*, 3–30, doi:10.1016/S0985-3111(01)01066-X.

Brousse, R., and H. Moine Vaziri (1982), L'association shoshonitique du Damavand, *Geol. Rundsch.*, *71*, 687–702, doi:10.1007/BF01822389.

Cañón-Tapia, E., and G. P. L. Walker (2004), Global aspects of volcanism: The perspectives of "plate tectonics" and "volcanic systems", *Earth Sci. Rev.*, *66*, 163–182, doi:10.1016/j.earscirev.2003.11.001.

Castillo, P. R. (2012), Adakite petrogenesis, *Lithos*, *134–135*, 304–316, doi:10.1016/j.lithos.2011.09.013.

Castro, A., and C. Fernandez (1998), Granite intrusion by externally induced growth and deformation of the magma reservoir, the example of the Plasenzuela pluton, Spain, *J. Struct. Geol.*, *20*, 1219–1228, doi:10.1016/S0191-8141(98)00056-X.

Chalot-Prat, F., and R. Girbacea (2000), Partial delamination of continental mantle lithosphere, uplift-related crust-mantle decoupling, volcanism and basin formation: A new model for the Pliocene-Quaternary evolution of the southern East-Carpathians, Romania, *Tectonophysics*, *327*, 83–107, doi:10.1016/S0040-1951(00)00155-4.

Chalot-Prat, F., T. J. Falloon, D. H. Green, and W. O. Hibberson (2010), An experimental study of liquid compositions in equilibrium with plagioclase + spinel lherzolite at low pressures (0•75GPa), *J. Petrol.*, *51*(11), 2349–2376, doi:10.1093/petrology/egq060.

Chiaradia, M., O. Muntener, B. Beate, and D. Fontignie (2009), Adakite-like volcanism of Ecuador: Lower crust magmatic evolution and recycling, *Contrib. Mineral. Petrol.*, *158*, 563–588, doi:10.1007/s00410-009-0397-2.

Copley, A., and J. Jackson (2006), Active tectonics of the Turkish-Iranian Plateau, *Tectonics*, *25*, TC6006, doi:10.1029/2005TC001906.

Corsaro, R. A., M. Neri, and M. Pompilio (2002), Paleo-environmental and volcano-tectonic evolution of the south-eastern flank of Mt. Etna during the last 225 ka inferred from volcanic succession of the "Timpe," Acireale, Sicily, *J. Volcanol. Geotherm. Res.*, *113*, 289–306, doi:10.1016/S0377-0273(01)00262-1.

Davidson, J. P., J. Hassanzadeh, R. Berzins, D. F. Stockli, B. Bashukooh, B. Turrin, and A. Pandamouz (2004), The geology of Damavand volcano, Alborz Mountains, northern Iran, *Geol. Soc. Am. Bull.*, *116*, 16–29, doi:10.1130/B25344.1.

Delaloye, M., and J. Desmons (1980), Ophiolites and melange terranes in Iran: A geochronological study and its paleotectonic implications, *Tectonophysics*, *68*, 83–111, doi:10.1016/0040-1951(80)90009-8.

Delaney, P. T., D. D. Pollard, J. L. Ziony, and E. H. McKee (1986), Field relations between dikes and joints: Emplacement processes and paleostress analysis, *J. Geophys. Res.*, *91*, 4920–4938, doi:10.1029/JB091iB05p04920.

Dewey, J. F., M. R. Hempton, W. S. F. Kidd, F. Saroglu, and A. M. C. Sengör (1986), Shortening of continental lithosphere: The neotectonics of eastern Anatolia—A young collision zone, in *Collosion Tectonics*, edited by M. P. Coward and A. C. Ries, *Geol. Soc. Spec. Publ.*, *19*, 3–36.

Dilek, Y. (2006), Collision tectonics of the Mediterranean region: Causes and consequences, in *Postcollisional Tectonics and Magmatism in the Mediterranean Region and Asia*, edited by Y. Dilrek and S. Pavlides, *Spec. Pap. Geol. Soc. Am.*, *409*, 1–13.

Dilek, Y., and E. M. Moores (1999), A Tibetan model for the early Tertiary western United States, *J. Geol. Soc.*, *156*, 929–941, doi:10.1144/gsjgs.156.5.0929.

Djamour, Y., et al. (2010), GPS and gravity constraints on continental deformation in the Alborz mountain range, Iran, *Geophys. J. Int.*, *183* (3), 1287–1301, doi:10.1111/j.1365-246X.2010.04811.x.

Doglioni, C., P. Harabaglia, S. Merlini, F. Mongelli, A. Peccerillo, and C. Piromallo (1999), Orogens and slabs vs their direction of subduction, *Earth Sci. Rev.*, *45*, 167–208, doi:10.1016/S0012-8252(98)00045-2.

Doglioni, C., F. Innocenti, and G. Mariotti (2001), Why Mt Etna?, *Terra Nova*, *13*, 25–31, doi:10.1046/j.1365-3121.2001.00301.x.

Doglioni, C., E. Carminati, M. Cuffaro, and D. Scrocca (2007), Subduction kinematics and dynamic constraints, *Earth Sci. Rev.*, *83*, 125–175, doi:10.1016/j.earscirev.2007.04.001.

Doglioni, C., S. Tonarini, and F. Innocenti (2009), Mantle wedge asymmetries and geochemical signatures along W- and E-NE-directed subduction zones, *Lithos*, *113*, 179–189, doi:10.1016/j.lithos.2009.01.012.

Drummond, M. S., and M. J. Defant (1990), A model for trondhjemite–tonalite–dacite genesis and crystal growth via slab melting: Archean to modern comparisons, *J. Geophys. Res.*, *95*, 21,503–21,521, doi:10.1029/JB095iB13p21503.

Ducea, M. H. (2011), Fingerprinting orogenic delamination, *Geology*, *39*, 191–192, doi:10.1130/focus022011.1.

Farbod, Y., O. Bellier, E. Shabanian, and M. R. Abbassi (2011), Geomorphic and structural variations along the Doruneh Fault System (central Iran), *Tectonics*, *30*, TC6014, doi:10.1029/2011TC002889.

Feraud, G., and R. Campredon (1983), Geochronology and structural study of Tertiary and Quaternary dikes in southern France and Sardinia: An example of utilization of dike swarms as paleostress indicators, *Tectonophysics*, *98*, 297–325, doi:10.1016/0040-1951(83)90299-8.

Feraud, G., I. Kaneoka, and J. C. Allègre (1980), K/Ar ages and stress pattern in the Azores: Geodynamic implications, *Earth Planet. Sci. Lett.*, *46*, 275–286, doi:10.1016/0012-821X(80)90013-8.

Fiske, R. S., and E. D. Jackson (1972), Orientation and growth of Hawaiian rifts: The effect of regional structure and gravitational stresses, *Proc. R. Soc. A*, *329*, 299–326, doi:10.1098/rspa.1972.0115.

Galland, O., E. Hallot, P. R. Cobbold, G. Ruffet, and J. de Bremond d'Ars (2007), Volcanism in a compressional Andean setting: A structural and geochronology study of Tromen volcano (Neuquen province), Argentina, *Tectonics*, *26*, TC4010, doi:10.1029/2006TC002011.

García Palomo, A., J. L. Macias, and J. M. Espindola (2004), Strike-slip faults and K-alkaline volcanism at El Chichon volcano, southeastern

Mexico, *J. Volcanol. Geotherm. Res.*, *136*, 247–268, doi:10.1016/j.jvolgeores.2004.04.001.

Ghaemi, F., F. Ghaemi, and K. Hosseini (1999), Geological map of Iran, Neyshabur sheet, *Map 7762*, scale 1:100,000, Geol. Surv. of Iran, Tehran.

Ghasemi, H., M. Sadeghian, A. R. Khan Alizadeh, and A. Tanha (2010), Petrology, geochemistry and radiometric ages of high silica adakitic domes of Neogene continental arc, south of Quchan [in Persian with English abstract], *Iran. J. Crystallogr. Mineral.*, *18*(3), 347–370.

Gibbons, W., and T. Moreno (2002), Tectonomagmatism in continental arcs: Evidence from the Sark arc complex, *Tectonophysics*, *352*, 185–201, doi:10.1016/S0040-1951(02)00196-8.

Gioncada, A., L. Vezzoli, R. Mazzuoli, R. Omarini, P. Nonnotte, and H. Guillou (2010), Pliocene intraplate-type volcanism in the Andean foreland at 26°10′S, 64°40′W (NW Argentina): Implications for magmatic and structural evolution of the Central Andes, *Lithosphere*, *2*, 153–171, doi:10.1130/L81.1.

Gök, R., E. Sandvol, N. Turkelli, D. Seber, and M. Barazangi (2003), Sn attenuation in the Anatolian and Iranian plateau and surrounding regions, *Geophys. Res. Lett.*, *30*(24), 8042, doi:10.1029/2003GL018020.

Green, D. H., T. J. Falloon, S. M. Eggin, and G. M. Yaxley (2001), Primary magmas and mantle temperatures, *Eur. J. Mineral.*, *13*, 437–451, doi:10.1127/0935-1221/2001/0013-0437.

Grib, E. N., V. L. Leonov, and A. B. Perepelov (2009), The Karymskii volcanic center: Volcanic rock geochemistry, *J. Volcanol. Seismol.*, *3*, 367–387, doi:10.1134/S0742046309060013.

Grocott, J., M. Brown, R. D. Dallmeyer, G. K. Taylor, and P. J. Treloar (1994), Mechanisms of continental growth in extensional arcs: An example from the Andean plate-boundary zone, *Geology*, *22*, 391–394, doi:10.1130/0091-7613(1994)022<0391:MOCGIE>2.3.CO;2.

Guest, B., G. J. Axen, P. S. Lam, and J. Hassanzadeh (2006), Late Cenozoic shortening in the west central Alborz mountains, northern Iran, by combined conjugate strike-slip and thin-skinned deformation, *Geosphere*, *2*, 35–52, doi:10.1130/GES00019.1.

Guest, B., B. K. Horton, G. J. Axen, J. Hassanzadeh, and W. C. McIntosh (2007), Middle to late Cenozoic basin evolution in the western Alborz Mountains: Implications for the onset of collisional deformation in northern Iran, *Tectonics*, *26*, TC6011, doi:10.1029/2006TC002091.

Gvirtzman, Z., and A. Nur (1999), The formation of Mount Etna as the consequence of slab rollback, *Nature*, *401*, 782–785, doi:10.1038/44555.

Haghipour, A., H. Taraz, and F. Vahdati Daneshmand (1986), Geological map of Iran, Tehran sheet, *Map F5*, scale 1:250 000, Geol. Surv. of Iran, Tehran.

Hedayati, A., J. L. Brander, and M. Berberian (1976), Microearthquake survey of Tehran region. Iran, *Bull. Seismol. Soc. Am.*, *66*, 1713–1725.

Hessami, K., H. Koyi, C. Talbot, H. Tabassi, and E. Shabanian (2001), Progressive unconformities within an evolving foreland fold-thrust belt, Zagros Mountains, *J. Geol. Soc.*, *158*, 969–981, doi:10.1144/0016-764901-007.

Hessami, K., F. Jamali, and H. Tabassi (2003), *The Map of Major Active Faults of Iran*, Int. Inst. of Earthquake Eng. and Seismol., Tehran.

Hollingsworth, J., M. Fattahi, R. Walker, M. Talebian, A. Bahroudi, M. J. Bolourchi, J. Jackson, and A. Copley (2010), Oroclinal bending, distributed thrust and strike-slip faulting, and the accommodation of Arabia-Eurasia convergence in NE Iran since the Oligocene, *Geophys. J. Int.*, *181*, 1214–1246, doi:10.1111/j.1365-246X.2010.04591.x.

Jackson, E. D., and H. R. Shaw (1975), Stress Fields in Central Portions of the Pacific Plate: Delineated in Time by Linear Volcanic Chains, *J. Geophys. Res.*, *80*, 1861–1874, doi:10.1029/JB080i014p01861.

Jackson, J. A., A. J. Haines, and W. E. Holt (1995), The accommodation of Arabia-Eurasia plate convergence in Iran, *J. Geophys. Res.*, *100*, 15,205–15,219, doi:10.1029/95JB01294.

Jackson, J., K. Priestley, M. Allen, and M. Berberian (2002), Active tectonics of the South Caspian Basin, *Geophys. J. Int.*, *148*, 214–245.

Jahangiri, A. (2007), Post-collisional Miocene adakitic volcanism in NW Iran: Geochemical and geodynamic implications, *J. Asian Earth Sci.*, *30*, 433–447, doi:10.1016/j.jseaes.2006.11.008.

Javidfakhr, B., O. Bellier, E. Shabanian, S. Ahmadian, and A. Saidi (2011a), Plio-Quaternary tectonic regime changes in the transition zone between Alborz and Kopeh Dagh mountain ranges (NE Iran), *Tectonophysics*, *506*, 86–108, doi:10.1016/j.tecto.2011.04.013.

Javidfakhr, B., O. Bellier, E. Shabanian, L. Siame, L. Léanni, D. Bourlès, and S. Ahmadian (2011b), Fault kinematics and active tectonics at the southeastern boundary of the eastern Alborz (Abr and Khij fault zones): Geodynamic implications for NNE Iran, *J. Geodyn.*, *52*(3–4), 290–303, doi:10.1016/j.jog.2011.02.005.

Kadinsky-Cade, K., M. Barazangi, J. Oliver, and B. Isacks (1981), Lateral variations of high frequency seismic wave propagation at regional distances across the Turkish and Iranian plateaus, *J. Geophys. Res.*, *86*, 9377–9396, doi:10.1029/JB086iB10p09377.

Karakhanian, A., R. Djrbashian, V. Trifonov, H. Philip, S. Arakelian, and A. Avagian (2002), Holocene historical volcanism and active faults as natural risk factors for Armenia and adjacent countries, *J. Volcanol. Geotherm. Res.*, *113*, 319–344, doi:10.1016/S0377-0273(01)00264-5.

Karakhanian, A., R. Jrbashyan, V. Trifonov, H. Philip, S. Arakelian, A. Avagyan, H. Baghdassaryan, V. Davtian, and Y. Ghoukassyan (2003), Volcanic hazards in the region of the Armenian nuclear power plant, *J. Volcanol. Geotherm. Res.*, *126*, 31–62, doi:10.1016/S0377-0273(03)00115-X.

Karakhanian, A. S., et al. (2004), Active faulting and natural hazards in Armenia, eastern Turkey and northwestern Iran, *Tectonophysics*, *380*, 189–219, doi:10.1016/j.tecto.2003.09.020.

Kaviani, A., D. Hatzfeld, A. Paul, M. Tatar, and K. Priestley (2009), Shear-wave splitting, lithospheric anisotropy, and mantle deformation beneath the Arabia-Eurasia collision zone in Iran, *Earth Planet. Sci. Lett.*, *286*, 371–378, doi:10.1016/j.epsl.2009.07.003.

Kay, R. W., and S. M. Kay (1993), Delamination and delamination magmatism, *Tectonophysics*, *219*, 177–189, doi:10.1016/0040-1951(93)90295-U.

Kelly, R. K., P. B. Kelemen, and M. Jull (2003), Buoyancy of the continental upper mantle, *Geochem. Geophys. Geosyst.*, *4*(2), 1017, doi:10.1029/2002GC000399.

Keskin, M. (2003), Magma generation by slab steepening and breakoff beneath a subduction-accretion complex: An alternative model for collision-related volcanism in Eastern Anatolia, Turkey, *Geophys. Res. Lett.*, *30*(24), 8046, doi:10.1029/2003GL018019.

Keskin, M. (2007), Eastern Anatolia: A hotspot in a collision zone without a mantle plume, in *Plates, Plumes, and Planetary Processes*, edited by G. R. Foulger and D. M. Jurdy, *Spec. Pap. Geol. Soc. Am.*, *430*, 693–722, doi:10.1130/2007.2430(32).

Keskin, M., J. A. Pearce, and J. G. Mitchell (1998), Volcano-stratigraphy and geochemistry of collision-related volcanism on the Erzurum-Kars Plateau, North Eastern Turkey, *J. Volcanol. Geotherm. Res.*, *85*, 355–404, doi:10.1016/S0377-0273(98)00063-8.

Kheirkhah, M., M. B. Allen, and M. Emami (2009), Quaternary syn-collision magmatism from the Iran/Turkey borderlands, *J. Volcanol. Geotherm. Res.*, *182*, 1–12, doi:10.1016/j.jvolgeores.2009.01.026.

Khodami, M., et al. (2009), Pliocene–Quaternary Adakite volcanism in the Isfahan area, Central Iranian magmatic belt, *Neues Jahrb. Mineral., Abh.*, *186*(3), 235–248.

Koçyigit, A., A. Yilmaz, S. Adamia, and S. Kuloshvili (2001), Neotectonics of East Anatolian Plateau (Turkey) and Lesser Caucasus: Implication for transition from thrusting to strike-slip faulting, *Geodin. Acta*, *14*, 177–195, doi:10.1016/S0985-3111(00)01064-0.

Lavenu, A., and J. Cembrano (1999), Compressional- and trasnpressional-stress pattern for Pliocene and Quanternary brittle deformation in fore arc and intra-arc zones (Andes of central and Southern Chile), *J. Struct. Geol.*, *21*, 1669–1691, doi:10.1016/S0191-8141(99)00111-X.

Lécuyer, F., O. Bellier, A. Gourgaud, and P. M. Vincent (1997), Tectonique active du Nord-Est de Sulawesi (Indonésie) et contrôle structural de la caldeira de Tondano, *C.R. Acad. Sci, Ser. IIA*, *325*, 607–613.

Le Dortz, K., et al. (2009), Holocene right-slip rate determined by cosmogenic and OSL dating on the Anar fault, Central Iran, *Geophys. J. Int.*, *179*(2), 700–710, doi:10.1111/j.1365-246X.2009.04309.x.

Lei, J., and D. Zhao (2007), Teleseismic evidence for a break-off subducting slab under Eastern Turkey, *Earth Planet. Sci. Lett.*, *257*, 14–28, doi:10.1016/j.epsl.2007.02.011.

Lensch, G., A. Mihn, and N. Alavi-Tehrani (1977), Petrography and geology of the ophiolite belt north of Sabzevar (Khorasan), Iran, *Neues Jahrb. Geol. Palaeontol. Abh.*, *131*, 156–178.

Liotard, J. M., J. M. Dautria, D. Bosch, M. Condomines, M. Mehdizadeh, and J.-F. Ritz (2008), Origin of the absarokite–banakite association of the Damavand volcano (Iran): Trace elements and Sr, Nd, Pb isotope constraints, *Int. J. Earth Sci.*, *97*, 89–102, doi:10.1007/s00531-006-0159-6.

Lyberis, N., and G. Manby (1999), Oblique to orthogonal convergence across the Turan block in the post-Miocene, *AAPG Bull.*, *83*(7), 1135–1160.

Macpherson, C. G., S. T. Dreher, and M. F. Thirlwall (2006), Adakites without slab melting: High pressure differentiation of island arc magma, Mindanao, the Philippines, *Earth Planet. Sci. Lett.*, *243*, 581–593, doi:10.1016/j.epsl.2005.12.034.

Maggi, A., and K. Priestley (2005), Surface waveform tomog raphy of the Turkish-Iranian plateau, *Geophys. J. Int.*, *160*, 1068–1080, doi:10.1111/j.1365-246X.2005.02505.x.

Maggi, M., J. Jackson, D. McKenzie, and K. Priestley (2000), Earthquake focal depths, effective elastic thickness, and the strength of the continental lithosphere, *Geology*, *28*, 495–498, doi:10.1130/0091-7613(2000)28<495:EFDEET>2.0.CO;2.

McCann, T., F. Chalot-Prat, and A. Saintot (2010), The Early Mesozoic evolution of the Western Greater Caucasus (Russia): Triassic–Jurassic sedimentary and magmatic history, in *Sedimentary Basin Tectonics From*

the Black Sea and Caucasus to the Arabian Platform, edited by M. Sosson et al., *Geol. Soc. Spec. Publ.*, *340*, 181–238, doi:10.1144/SP340.10.

McClusky, S., et al. (2000), Global Positioning System constraints on plate kinematics and dynamics in the eastern Mediterranean and Caucasus, *J. Geophys. Res.*, *105*, 5695–5719, doi:10.1029/1996JB900351.

McDermott, F., F. G. Delfin, M. J. Defant, S. Turner, and R. Maury (2005), The petrogenesis of volcanics from Mt. Bulusan and Mt. Mayon in the Bicol arc, the Philippines, *Contrib. Mineral. Petrol.*, *150*, 652–670, doi:10.1007/s00410-005-0042-7.

McDonough, W. F., and S. S. Sun (1995), The composition of the Earth, *Chem. Geol.*, *120*(3–4), 223–253, doi:10.1016/0009-2541(94)00140-4.

McNulty, B., D. Farber, G. S. Wallace, R. Lopez, and O. Palacios (1998), Role of plate kinematics and plate-slip-vector partitioning in continental magmatic arcs: Evidence from the Cordillera Blanca, Peru, *Geology*, *26*, 827–830, doi:10.1130/0091-7613(1998)026<0827:ROPKAP>2.3.CO;2.

Mehdizadeh, H., J.-M. Liotard, and J.-M. Dautria (2002), Geochemical characteristics of an intracontinental shoshonitic association: The example of the Damavand volcano, Iran, *C. R. Geosci.*, *334*(2), 111–117, doi:10.1016/S1631-0713(02)01717-0.

Mirnejad, H., J. Hassanzadeh, B. L. Cousens, and B. E. Taylor (2010), Geochemical evidence for deep mantle melting and lithospheric delamination as the origin of the inland Damavand volcanic rocks of northern Iran, *J. Volcanol. Geotherm. Res.*, *198*, 288–296, doi:10.1016/j.jvolgeores.2010.09.014.

Moinabadi, M. E., and A. Yassaghi (2007), Geometry and kinematics of the Mosha Fault, south central Alborz Range, Iran: An example of basement involved thrusting, *J. Asian Earth Sci.*, *29*, 928–938, doi:10.1016/j.jseaes.2006.07.002.

Monaco, C., P. Tapponnier, L. Tortorici, and P. Y. Gillot (1997), Late Quaternary slip rates on the Acireale-Piedimonte normal faults and tectonic origin of Mt. Etna (Sicily), *Earth Planet. Sci. Lett.*, *147*, 125–139, doi:10.1016/S0012-821X(97)00005-8.

Morand, V. J. (1992), Pluton emplacement in a strike-slip fault zone: The Doctors Flat Pluton, Victoria, Australia, *J. Struct. Geol.*, *14*, 205–213, doi:10.1016/0191-8141(92)90057-4.

Moreau, C., D. Demaiffe, Y. Bellion, and A. M. Boullier (1994), A tectonic model for the location of the Palaeozoic ring complexes in Air (Niger, West Africa), *Tectonophysics*, *234*, 129–146, doi:10.1016/0040-1951(94)90208-9.

Morley, C., B. Kongwung, A. A. Julapour, M. Abdolghafourian, M. Hajian, D. Waples, J. Warren, H. Otterdoom, K. Srisuriyon, and H. Kazemi (2009), Structural development of the major Late Cenozoic basin and transpressional belt in Central Iran: The Central Basin in the Qom-Saveh area, *Geosphere*, *5*, 325–362, doi:10.1130/GES00223.1.

Moune, S., O. Sigmarsson, T. Thordarson, and P. J. Gauthier (2007), Recent volatile evolution in the magmatic system of Hekla volcano, Iceland, *Earth Planet. Sci. Lett.*, *255*, 373–389, doi:10.1016/j.epsl.2006.12.024.

Mount, V. S., and J. Suppe (1992), Present-day stress orientations adjacent to active strike-slip faults: California and Sumatra, *J. Geophys. Res.*, *97*, 11,995–12,031, doi:10.1029/92JB00130.

Mouthereau, F., J. Tensi, N. Bellahsen, O. Lacombe, T. De Boisgrollier, and S. Kargar (2007), Tertiary sequence of deformation in a thin-skinned/thick-skinned collision belt: The Zagros folded belt (Fars, Iran), *Tectonics*, *26*, TC5006, doi:10.1029/2007TC002098.

Mouthereau, F., O. Lacombe, and J. Vergés (2012), Building the Zagros collisional orogen: Timing, strain distribution and the dynamics of Arabia/Eurasia plate convergence, *Tectonophysics*, *532–535*, 27–60, doi:10.1016/j.tecto.2012.01.022.

Muller, O. H., and D. D. Pollard (1977), The stress state near Spanish Peaks, Colorado, determined from a dike pattern, *Pure Appl. Geophys.*, *115*, 69–86, doi:10.1007/BF01637098.

Nakamura, K. (1977), Volcanoes as possible indicators of tectonic stress orientation: Principle and proposal, *J. Volcanol. Geotherm. Res.*, *2*, 1–16, doi:10.1016/0377-0273(77)90012-9.

Nakamura, K., K. H. Jacobs, and J. N. Davies (1977), Volcanoes as possible indicators of tectonic stress orientations - Aleutian and Alaska, *Pure Appl. Geophys.*, *115*, 87–112, doi:10.1007/BF01637099.

Nazari, H. (2006), Analyse de la tectonique récente et active dans l'Alborz Central et la région de Téhéran: Approche morphotectonique et paléoseismologique, PhD thesis, 246 pp., Fac. des Sci. et des Tech. du Languedoc, Univ. Montpellier II, Montpellier, France.

Nazari, H., J.-F. Ritz, A. Shafei, A. Ghassemi, R. Salamati, J. L. Michelot, and M. Massault (2009), Morphological and paleoseismological analyses of the Taleghan fault, Alborz, Iran, *Geophys. J. Int.*, *178*, 1028–1041, doi:10.1111/j.1365-246X.2009.04173.x.

Nemati, M., D. Hatzfeld, M. R. Gheitanchi, A. Sadidkhouy, and N. Mirzaei (2011), Microseismicity and seismotectonics of the Firuzkuh and Astaneh faults (East Alborz, Iran), *Tectonophysics*, *506*, 11–21, doi:10.1016/j.tecto.2011.04.007.

Paul, A., A. Kaviani, D. Hatzfeld, J. Vergne, and M. Mokhtari (2006), Seismological evidence for crustal-scale thrusting in the Zagros mountain belt (Iran), *Geophys. J. Int.*, *166*, 227–237, doi:10.1111/j.1365-246X.2006.02920.x.

Peacock, S. M., T. Rushmer, and A. B. Thompson (1994), Partial melting of subducting oceanic crust, *Earth Planet. Sci. Lett.*, *121*, 227–244, doi:10.1016/0012-821X(94)90042-6.

Pearce, J. A., J. F. Bender, S. E. De Long, W. S. F. Kidd, P. J. Low, Y. Guner, F. Saroglu, Y. Yilmaz, S. Moorbath, and J. G. Mitchell (1990), Genesis of collision volcanism in eastern Anatolia, Turkey, *J. Volcanol. Geotherm. Res.*, *44*, 189–229, doi:10.1016/0377-0273(90)90018-B.

Radjaee, A., D. Rham, M. Mokhtari, M. Tatar, K. Priestley, and D. Hatzfeld (2010), Variation of Moho depth in the central part of the Alborz Mountains, northern Iran, *Geophys. J. Int.*, *181*, 173–184, doi:10.1111/j.1365-246X.2010.04518.x.

Rahimi, H., K. Mothaghi, S. Mukhopadhyay, and H. Hamzehloo (2010), Variation of coda wave attenuation in the Alborz region and central Iran, *Geophys. J. Int.*, *181*, 1645–1654.

Regard, V., et al. (2005), Cumulative right-lateral fault slip rate across the Zagros–Makran transfer zone: Role of the Minab–Zendan fault system in accommodating Arabia–Eurasia convergence in southeast Iran, *Geophys. J. Int.*, *162*, 177–203, doi:10.1111/j.1365-246X.2005.02558.x.

Reilinger, R., et al. (2006), GPS constraints on continental deformation in the Africa-Arabia-Eurasia continental collision zone and implications for the dynamics of plate interactions, *J. Geophys. Res.*, *111*, B05411, doi:10.1029/2005JB004051.

Riller, U., I. A. Petrinovic, J. Ramelow, J. Grekowiak, M. Strecker, and O. Onken (2001), Late Cenozoic tectonism, caldera and plateau formation in the central Andes, *Earth Planet. Sci. Lett.*, *188*, 299–311, doi:10.1016/S0012-821X(01)00333-8.

Ritz, J.-F., et al. (2003), Determining the long-term slip rate along the Mosha Fault, Central Alborz, Iran, Implications in terms of seismic activity, paper presented at 4th International Conference of Seismology and Earthquake Engineering, Int. Inst. of Earthquake Eng. and Seismol., Tehran.

Ritz, J.-F., H. Nazari, R. Salamati, A. Shafeii, S. Solaymani, and P. Vernant (2006), Active transtension inside Central Alborz: A new insight into the Northern Iran–Southern Caspian geodynamics, *Geology*, *34*, 477–480, doi:10.1130/G22319.1.

Rodgers, A. J., J. F. Ni, and T. M. Hear (1997), Propagation characteristics of short-period *Sn* and *Lg* in the Middle East, *Bull. Seismol. Soc. Am.*, *87*, 396–413.

Saadat, S., M. H. Karimpour, and C. Stern (2010), Petrochemical characteristics of Neogene and Quaternary alkali olivine basalts from the Western Margin of the Lut Block, Eastern Iran, *Iran. J. Earth Sci.*, *2*, 87–106.

Sandwell, D. T., D. Anderson, and P. Wessel (2005), Global tectonic maps, in *Plates, Plumes and Paradigms*, edited by G. L. Foulger et al., *Spec. Pap. Geol. Soc. Am.*, *388*, 1–10, doi:10.1130/0-8137-2388-4.1.

Santacroce, R. (Ed.) (1987), *Somma-Vesuvius*, *Quad. Ric. Sci.*, *114*, 251 pp.

Şengör, A. M. C., S. Ozeren, T. Genc, and E. Zor (2003), East Anatolian high plateau as a mantle supported, north south shortened domal structure, *Geophys. Res. Lett.*, *30*(24), 8045, doi:10.1029/2003GL017858.

Shabanian, E., L. Siame, O. Bellier, L. Benedetti, and M. R. Abbassi (2009a), Quaternary slip-rates along the north-eastern boundary of the Arabia-Eurasia collision zone (Kopeh Dagh Mountains, North-East Iran), *Geophys. J. Int.*, *178*, 1055–1077, doi:10.1111/j.1365-246X.2009.04183.x.

Shabanian, E., O. Bellier, L. Siame, N. Arnaud, M. R. Abbassi, and J. J. Cochemé (2009b), New tectonic configuration in NE Iran: Active strike-slip faulting between the Kopeh Dagh and Binalud mountains, *Tectonics*, *28*, TC5002, doi:10.1029/2008TC002444.

Shabanian, E., O. Bellier, M. R. Abbassi, L. L. Siame, and Y. Farbod (2010), Plio-Quaternary stress states in NE Iran: Kopeh Dagh and Allah Dagh-Binalud mountains, *Tectonophysics*, *480*, 280–304, doi:10.1016/j.tecto.2009.10.022.

Shad Manaman, N., H. Shomali, and H. Koyi (2011), New constraints on upper-mantle S-velocity structure and crustal thickness of the Iranian plateau using partitioned waveform inversion, *Geophys. J. Int.*, *184*, 247–267, doi:10.1111/j.1365-246X.2010.04822.x.

Shirzaei, M., T. R. Walter, H. R. Nankali, and E. P. Holohan (2011), InSAR time series Gravity-driven deformation of Damavand volcano, Iran, detected through, *Geology*, *39*, 251–254, doi:10.1130/G31779.1.

Shojaat, B., A. A. Hassanipak, K. Mobasher, and A. M. Ghazi (2003), Petrology, geochemistry and tectonics of the Sabzevar ophiolite, North Center Iran, *J. Asian Earth Sci.*, *21*, 1053–1067, doi:10.1016/S1367-9120(02)00143-8.

Sodoudi, F., X. Yuan, R. Kind, B. Heit, and A. Sadidkhouy (2009), Evidence for a missing crustal root and a thin lithosphere beneath the Central Alborz by receiver function studies, *Geophys. J. Int.*, *177*(2), 733–742, doi:10.1111/j.1365-246X.2009.04115.x.

Solaymani, S., K. Feghhi, E. Shabanian, M. R. Abbassi, and J.-F. Ritz (2003), *Preliminary paleoseismological studies on the Mosha Fault at Mosha Valley [in Persian]*, 89 pp., Int. Inst. of Earthquake Eng. and Seismol., Tehran.

Solaymani Azad, S. (2009), Evaluation de l'aléa sismique pour les villes de Téhéran, Tabriz et Zandjan dans le NW de l'Iran. Approche morphotectnique et paléosismologique, PhD thesis, 150 pp., Univ. Montpellier II, Montpellier, France.

Solaymani Azad, S., S. Dominguez, H. Philip, K. Hessami, M. R. Forutan, M. Shahpasan Zadeh, and J.-F. Ritz (2011a), The Zandjan fault system: Morphological and tectonic evidences of a new active fault network in the NW of Iran, *Tectonophysics*, *506*, 73–85, doi:10.1016/j.tecto.2011.04.012.

Solaymani Azad, S., J.-F. Ritz, and M. R. Abbassi (2011b), Left-lateral active deformation along the Mosha–North Tehran fault system (Iran): Morphotectonics and paleoseismological investigations, *Tectonophysics*, *497*, 1–14, doi:10.1016/j.tecto.2010.09.013.

Spies, O., G. Lensch, and A. Mihem (1983), Geochemistry of the post-ophiolitic Tertiary volcanics between Sabzevar and Quchan (NE Iran), *Rep. Geol. Min. Surv. Iran*, *51*, 247–266.

Stampfli, G. M., and G. D. Borel (2002), A plate tectonic model for the Paleozoic and Mesozoic constrained by dynamic plate boundaries and restored synthetic oceanic isochrones, *Earth Planet. Sci. Lett.*, *196*, 17–33, doi:10.1016/S0012-821X(01)00588-X.

Stern, R. J. (2002), Subduction zones, *Rev. Geophys.*, *40*(4), 1012, doi:10.1029/2001RG000108.

Stöcklin, J. (1968), Structural history and tectonics of Iran, A review, *Am. Assoc. Pet. Geol. Bull.*, *52*(7), 1229–1258.

Stöcklin, J. (1974), Northern Iran: Alborz Mountains, in *Mesozoic–Cenozoic Belts*, edited by A. M. Spencer, *Spec. Publ. Geol. Soc. London*, *4*, 213–234.

Sun, S. S., and W. F. McDonough (1989), Chemical and isotopic systematics of oceanic basalts: Implications for mantle composition and processes, in *Magmatism in the Ocean Basins*, edited by A. D. Saunders and M. J. Norry, *Geol. Soc. Spec. Publ.*, *42*, 313–345.

Tabatabai, M. S., E. Bergman, and M. R. Gheitanchi (2008), 3–Dimensional upper mantle velocity structure for Iranian Plateau revealed by Pn and Sn tomography, *J. Earth Space Phys.*, *33*(3), 13–24.

Takada, A., Y. Ishizuka, S. Nakano, T. Yamamoto, M. Kobayashi, and Y. Suzuki (2007), Characteristic and evolution inferred from eruptive fissures of Fuji volcano, Japan, in *Fuji Volcano*, edited by S. Aramaki, pp. 183–202, Volcanol. Soc., Tokyo.

Talebian, M., and J. Jackson (2002), Offset on the Main Recent Fault of NW Iran and implications for the late Cenozoic tectonics of the Arabia–Eurasia collision zone, *Geophys. J. Int.*, *150*, 422–439, doi:10.1046/j.1365-246X.2002.01711.x.

Tatar, M., and D. Hatzfeld (2009), Microseismic evidence of slip partitioning for the Rudbar-Tarom earthquake (Ms 7.7) of 1990 June 20 in NW Iran, *Geophys. J. Int.*, *176*, 529–541, doi:10.1111/j.1365-246X.2008.03976.x.

Tatar, M., J. Jackson, D. Hatzfeld, and E. Bergman (2007), The 28 May 2004 Baladeh earthquake (Mw 6.2) in the Alborz, Iran: Implications for the geology of the South Caspian Basin margin and for the seismic hazard of Tehran, *Geophys. J. Int.*, *170*, 249–261, doi:10.1111/j.1365-246X.2007.03386.x.

Tchalenko, J. S. (1975), Seismicity and structure of the Kopet Dagh (Iran, USSR), *Philos. Trans. R. Soc., Ser. A*, *278*, 1–28, doi:10.1098/rsta.1975.0019.

Tchalenko, J. S., M. Berberian, H. Iranmanesh, M. Bailly, and M. Arsovsky (1974), Tectonic framework of the Tehran region, *Rep. Geol. Surv. Iran*, *29*, 7–46.

Tibaldi, A. (1992), The role of transcurrent intra-arc tectonics in the configuration of a volcanic arc, *Terra Nova*, *4*, 567–577, doi:10.1111/j.1365-3121.1992.tb00598.x.

Tibaldi, A. (2005), Volcanism in compressional tectonic settings. Is it possible?, *Geophys. Res. Lett.*, *32*, L06309, doi:10.1029/2004GL021798.

Tilling, R. I., T. L. Wight, and H. T. Millard (1987), Trace-element chemistry of Kilauea and Mauna Loa lava in space and time: A reconnaissance, in *Volcanism in Hawaii*, edited by R. W. Decker, T. L. Wright, and P. H. Stauffer, *USGS Prof. Pap.*, *1350*, 641–690.

Toksöz, M. N., and P. Bird (1977), Formation and evolution of marginal basins and continental plateaus, in *Island Arcs, Deep Sea Trenches and Back-Arc Basins*, edited by M. Talwani and W. C. Pitman III, *Maurice Ewing Ser*, 1, pp. 379–393, AGU, Washington, D. C., doi:10.1029/ME001p0379.

Topuz, G., A. I. Okay, R. Altherr, W. H. Schwarz, W. Siebel, T. Zack, M. Satır, and C. Şen (2011), Post-collisional adakite-like magmatism in the Ağvanis Massif and implications for the evolution of the Eocene magmatism in the Eastern Pontides (NE Turkey), *Lithos*, *125*, 131–150, doi:10.1016/j.lithos.2011.02.003.

Trifonov, V. G., K. Hessami, and F. Jamali (1996), West-Trending Oblique Sinitral-Reverse Fault system in Northern Iran, *Spec. Publ. 75*, Int. Inst. of Earthquake Eng. and Seismol., Tehran.

Vahdati Daneshmand, F. (1991), Geological map of Iran, Amol sheet, *Map F4*, scale 1:250 000, Geol. Surv. of Iran, Tehran.

Vernant, P., F. Nilforoushan, J. Chéry, R. Bayer, Y. Djamour, F. Masson, H. Nankali, J.-F. Ritz, M. Sedighi, and F. Tavakoli (2004), Deciphering oblique shortening of central Alborz in Iran using geodetic data, *Earth Planet. Sci. Lett.*, *223*, 177–185, doi:10.1016/j.epsl.2004.04.017.

Vezzoli, L., and V. Acocella (2009), Easter Island, SE Pacific: An end-member type of hotspot volcanism, *Geol. Soc. Am. Bull.*, *121*, 869–886, doi:10.1130/B26470.1.

Vigneresse, J. L. (1995), Control of granite emplacement by regional deformation, *Tectonophysics*, *249*, 173–186, doi:10.1016/0040-1951(95)00004-7.

Vincent, S. J., M. B. Allen, A. D. Ismail-Zadeh, R. Flecker, K. A. Foland, and M. D. Simmons (2005), Insights from the Talysh of Azerbaijan into the Paleogene evolution of the south Caspian region, *Geol. Soc. Am. Bull.*, *117*, 1513–1533, doi:10.1130/B25690.1.

Wagner, R., C. L. Rosenberg, M. R. Handy, C. Mobus, and M. Albertz (2006), Fracture-driven intrusion and upwelling of a mid-crustal pluton fed from a transpressive shear zone–the Riederferner pluton (Eastern Alps), *Geol. Soc. Am. Bull.*, *118*, 219–237, doi:10.1130/B25842.1.

Walker, R., and J. Jackson (2004), Active tectonics and Late Cenozoic strain distribution in central and eastern Iran, *Tectonics*, *23*, TC5010, doi:10.1029/2003TC001529.

White, S. M., J. A. Crisp, and F. J. Spera (2006), Long-term volumetric eruption rates and magma budgets, *Geochem. Geophys. Geosyst.*, *7*, Q03010, doi:10.1029/2005GC001002.

Yassaghi, A., and S. Madanipour (2008), Influence of a transverse basement fault on along-strike variations in the geometry of an inverted normal fault: Case study of the Mosha Fault, Central Alborz Range, Iran, *J. Struct. Geol.*, *30*, 1507–1519, doi:10.1016/j.jsg.2008.08.006.

Yilmaz, Y., Y. Guner, and F. Saroglu (1998), Geology of the Quaternary volcanic centres of the East Anatolia, *J. Volcanol. Geotherm. Res.*, *85*, 173–210, doi:10.1016/S0377-0273(98)00055-9.

Yokoyama, T., F. T. Aka, M. Kusakabe, and E. Nakamura (2007), Plume-lithosphere interaction beneath Mt. Cameroon volcano, Wes Africa: Constraints from ^{238}U-^{230}Th-^{226}Rn and Sr-Nd-Pb isotope ratios, *Geochim. Cosmochim. Acta*, *71*, 1835–1854, doi:10.1016/j.gca.2007.01.010.

Zanchi, A., F. Berra, M. Mattei, M. R. Ghassemi, and J. Sabouri (2006), Inversion tectonics in central Alborz, Iran, *J. Struct. Geol.*, *20*, 1–15.

Zoback, M. L., and M. Zoback (1980), State of stress in the conterminous United States, *J. Geophys. Res.*, *85*, 6113–6156, doi:10.1029/JB085iB11p06113.